Table of Contents

Table of Figures

Table of Tables

1 General Overview

1.1 Introduction

This document describes the three-dimensional (3D) water modeling system MOHID. The MOHID system includes a baroclinic hydrodynamic module for the water column and a 3D for the sediments and the correspondent eulerian transport and lagrangian transport modules. Parameters and processes involving non-conservative properties are object of specific modules (e.g. turbulence module, water quality, ecology and oil transformation). The turbulence module uses the well known GOTM[1] turbulence model.

The model is being developed by a large team from Instituto Superior Técnico[2] in close cooperation with Hidromod[3] Lda and includes contributions from the permanent research h team and from a large number of Ph.D students on Environmental and Mechanical Engineering and from IST master course on Modelling of the Marine Environment. Contributions form other research groups have also been very important for the development of the model.

The architecture of the model is presently coordinated by Ramiro Neves, Frank Braunschweig and Paulo Leitão[4]. The engineering of the model is mainly a responsibility of Paulo Leitão, Frank Braunschweig, Pedro Pina, Luis Fernandes, Rodrigo Fernandes and Pedro Chambel Leitão and Manuel Villarreal and Pedro Montero. The main contributors for the concepts included in the model and for model validation and operationality are Ramiro Neves, Adélio Silva, José Leitão, Flávio Martins and Aires dos

[1] GOTM (General Ocean Turbulence Model – http://www.gotm.net/

[2] Av. Rovisco Pais, 1049-001 Lisboa, Portugal. (http://ist.utl.pt).

[3] Sala 349, Núcleo Central do TagusPark, 2780-982, Porto Salvo, Portugal (http://www.hidromod.pt).

[4] Ricardo Miranda, a former member of this group also gave an important contribution for model architecture and engineering.

Santos. A loto of other people gave contributions that all together have strongly influenced the development of MOHID.

1.2 History

The development of MOHID started back in 1985, passing since this time through continuously updates and improvements due to its use in the framework of many research and engineering projects. Initially MOHID was a bi-dimensional tidal model by Neves, [1985]. This model was used to study estuaries and coastal areas using a classical finite-difference approach. In the subsequent years, bi-dimensional eulerian and lagrangian transport modules were included in this model, as well as a Boussinesq model for non-hydrostatic gravity waves by Silva, [1992]. The first three-dimensional model was introduced by Santos, [1995], which used a vertical double Sigma coordinate (MOHID 3D). The limitations of the double Sigma coordinate revealed the necessity to develop a model which could use a generic vertical coordinate, permitting the user to choose from several coordinates, depending of the main processes in the study area. With this Due to this necessity the concept of finite volumes was introduced with the version *Mesh 3D* by Martins, [1999]. In the *Mesh 3D* model, a 3D eulerian transport model, a 3D lagrangian transport model Leitão, [1996] and a zero-dimensional water quality model (Miranda, 1999) were included. This version of the model revealed that the use of an integrated model based on a generic vertical coordinate is a very powerful tool. However it was verified that the model was difficult to maintain and to extend due the limitations of the FORTRAN 77 language. Then it was decided to reorganize the model using FORTRAN 95 and an object oriented strategy.

1.3 Actual State

With the growing model complexity, it was necessary to introduce a new way in the organization of the information of the *Mohid* model. In 1998 the whole code was submitted to a complete rearrangement, using new the feature of programming languages and also the capacities of the computer to reprogram the whole *Mohid* model. The main goal of this rearrangement was to turn the model more robust, reliable and protect its structure against

involuntary programming errors, so it would be more easily “grow able”. To achieve this goal, objected oriented programming in FORTRAN was introduced to the *Mohid* model, like described in Decyk (Decyk, *et al*., 1997).

The philosophy of the new *Mohid* model (Miranda, *et al*., 2000), further on simple designated *Mohid*, permits to use the model in any dimension (one-dimensional, two-dimensional or three-dimensional). The whole model is programmed in ANSI FORTRAN 95, using the objected orientated philosophy. The subdivision of the program into modules, like the information flux between these modules was object of a study by the *Mohid* authors.

Actually the model *Mohid* is composed by over 40 modules which complete over 150 mil code lines. Each module is responsible to manage a certain kind of information. The main modules are the modules listed in Table 1-1.

Another important feature of *Mohid* is the possibility to run nested models. This feature enables the user to study local areas, obtaining the boundary conditions from the “father” model. The number of nested models is just limited by the available computer power.

Module Name	*Module Description*
Model	Manages the information flux between the hydrodynamic module and the two transport modules and the communication between nested models.
Hydrodynamic	Full 3D dimensional baroclinic hydrodynamic free surface model. Computes the water level, velocities and water fluxes.
Water Properties (Eulerian Transport)	Eulerian transport model. Manages the evolution of the water properties (temperature, salinity, oxygen, etc.) using a eulerian approach.
Lagrangian	Lagrangian transport model. Manages the evolution of

	the same properties as the water properties module using a lagrangian approach. Can also be used to simulate oil dispersion.
Water Quality	Zero-dimensional water quality model. Simulates the oxygen, nitrogen and phosphorus cycle. Used by the eulerian and the lagrangian transport modules. Based on a model initially developed by EPA (Bowie, *et. al.,* 1985).
Oil Dispersion	Oil dispersion module. Simulates the oil spreading due thickness gradients and internal oil processes like evaporation, emulsification, dispersion, dissolution and sedimentation.
Turbulence	One-dimensional turbulence model. Uses the formulation from the GOTM model.
Geometry	Stores and updates the information about the finite volumes.
Surface	Boundary conditions at the top of the water column.
Bottom	Boundary conditions at the bottom of the water column.
Open Boundary	Boundary conditions at the frontier with the open sea.
Discharges	River or Anthropogenic Water Discharges
Hydrodynamic File	Auxiliary module to store the hydrodynamic solution in an external file for posterior usage.

Table 1-1: Principal modules of the model Mohid

1.4 Applications

The MOHID model has been applied to several coastal and estuarine areas and it has showed its ability to simulate complex features of the flows. Several different coastal areas have been modeled with MOHID in the framework of research and consulting projects. Along the Portuguese

coast, different environments have been studied, including the main estuaries (Minho, Lima, Douro, Mondego, Tejo, Sado, Mira, Arade and Guadiana) and coastal lagoons (Ria de Aveiro and Ria Formosa), INAG [2001]; Martins et al. (2000). The model has been also implemented in most Galician Rías: Ría de Vigo by Taboada *et al*., (1998), Montero, (1999) and Montero *et al*. [1999], Ría de Pontevedra by Taboada *et al.* [2000] and Villarreal *et al.* [2000] and in other Rías by Pérez Villar *et al* [1999].

Far from the Atlantic coast of the Iberian Peninsula, some European estuaries have been modeled - Western Scheldt , The Netherlands, Gironde, France by Cancino and Neves, [1999] and Carlingford, Ireland, by Leitão, [1997] - as well as some estuaries in Brasil (Santos SP and Fortaleza).

Regarding to open sea, MOHID has been applied to the North-East Atlantic region where some processes including the Portuguese coastal current, Coelho *et al.* (1994), the slope current along the European Atlantic shelf break, Neves *et al*. (1998) and the generation of internal tides, Neves *et al*. (1998) have been studied and also to the Mediterranean Sea to simulate the seasonal cycle, Taboada, (1999) or the circulation in the Alboran Sea, Santos, (1995).

More recently MOHID has been applied to the several Portuguese fresh water reservoirs Monte Novo, Roxo and Alqueva, (Braunschweig, 2001), in order to study the flow and water quality.

2 The Model Module

2.1 Introduction

The module Model is the topmost module of the *Mohid* water modeling system and has two main responsibilities, the coordinates of the execution of the hydrodynamic module and the transport modules and the coordination of the father-son communication between nested models. Figure 2-1 shows this coordination.

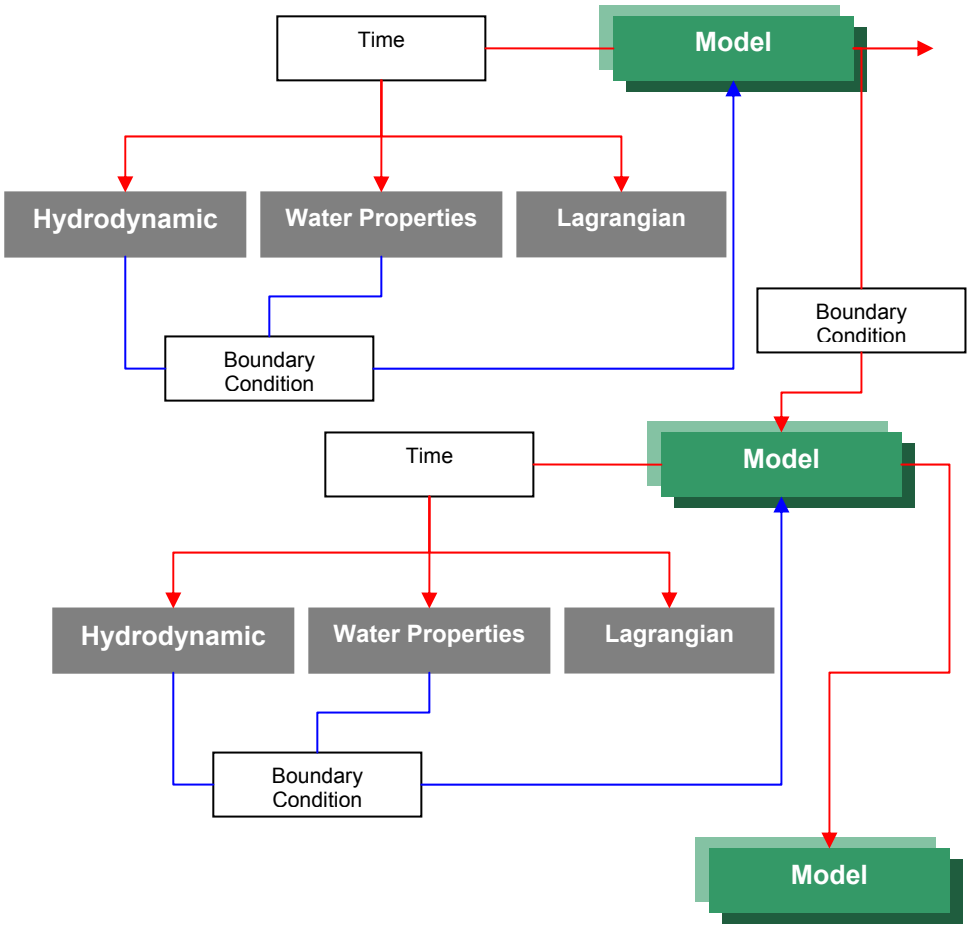

Figure 2-1: Information flux between the nested models

2.2 Coordination of the execution of one model

The coordination of the execution of one model consists of the actualization of the global model time and the update of the hydrodynamic

module and the transport models within one model. The transport modules can run with different time steps of the hydrodynamic module (since the time steps of the transport modules are multiplies of the hydrodynamic time step).

2.3 Coordination of the father son communication

The coordination of the information flux between the nested models includes the synchronization between different nested models, once nested models can also run with different time steps. The coordination of the nested models is done in a hierarchical way. Every model can have one or more nested child models, which recursively can have one or more child models. All the communication is done in one way direction, passing the boundary conditions from the father model to the son(s) model(s).

3 The Bathymetry Module

3.1 Introduction

The module Bathymetry is one of the lowest modules of the *Mohid* water modeling system. It has basically reads the bathymetric data from an ASCII input file and publishes this data to all client modules.

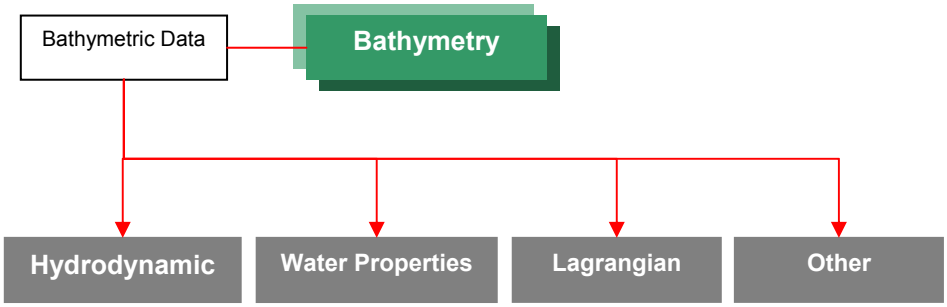

Figure 3-1: Information flux between the module bathymetry and other modules

The bathymetric data can be stored in any regular grid, with variable spacing along the X and the Y direction. For every grid point the depth of this point must be given. The horizontal coordinates can be supplied in different types of coordinates. Most common used are metric coordinates and geographic coordinates.

4 The Geometry Module

4.1 Introduction

The Geometry Module computes the lateral areas and volumes of the finite volume, based upon the surface elevation and the bathymetric data. This information is updated as needed, and published to the other modules of the *Mohid* model. Figure 4-1 represents the information flux between the geometry module and other modules.

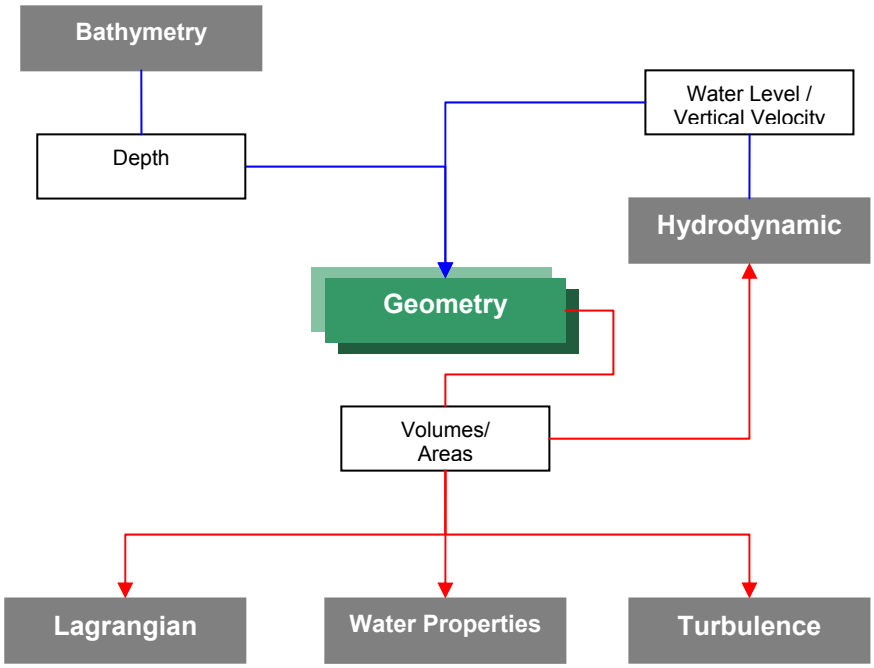

Figure 4-1: Information flux between the Geometry Module and other modules

4.2 Finite Volume

The model *Mohid* uses a finite volume approach (Chippada et al. [1998]; Martins et al. [1999], [2000]) to discretize the equations. In this approach, the discrete form of the governing equations is applied macroscopically to a cell control volume. A general conservation law for a scalar U, with sources Q in a control volume Ω is then written as:

$$\partial_t \int_{\Omega} U d\Omega + \oint_{S} \vec{F} d\vec{S} = \int_{\Omega} Q d\Omega \qquad \text{Eq. 4-1}$$

where *F* are the fluxes of the scalar through the surface *S* embedding the volume. After discretizing this expression in a cell control volume Ω_j where U_j is defined, we obtain:

$$\partial_t (U_j \Omega_j) + \sum_{faces} \vec{F} \cdot \vec{S} = Q_j \Omega_j \qquad \text{Eq. 4-2}$$

In this way, the procedure for solving the equations is independent of cell geometry. Actually, the cell can have any shape with only some constraints (see *Montero [1999]* or *Martins [2000]*) since only fluxes among cell faces are required. Therefore, a complete separation between physical variables and geometry is achieved (*Hirsch, [1988]*). As volumes can vary in the course of the calculus, geometry is updated in every time step after computing the physical variables. Moreover, the spatial coordinates are independent, and any geometry can be chosen for every dimension. Cartesian or curvilinear coordinates can be used in the horizontal and a generic vertical coordinate with different sub-domains can be used in the vertical. This general vertical coordinate allows minimizing the errors of some of the classical vertical coordinates (Cartesian, sigma, isopycnal) as pointed in (*Martins et al. [2000]*).

The volume element used in the model MOHID is shown in Figure 4-2. Only a vertical degree of freedom is allowed, and the grid is Cartesian orthogonal in the horizontal. The grid is staggered in the horizontal in an Arakawa C (*Arakawa and Lamb, [1977])* manner, i.e. horizontal velocities are located in the center of the west (u-velocity) and south (v-velocities) faces, while elevation, turbulent magnitudes and tracers are placed in the center. Also a staggering in the vertical is used, with vertical velocity w, tracers and turbulent magnitudes vertically placed in the top and bottom faces and horizontal velocities and elevation in the center of the element (in vertical).

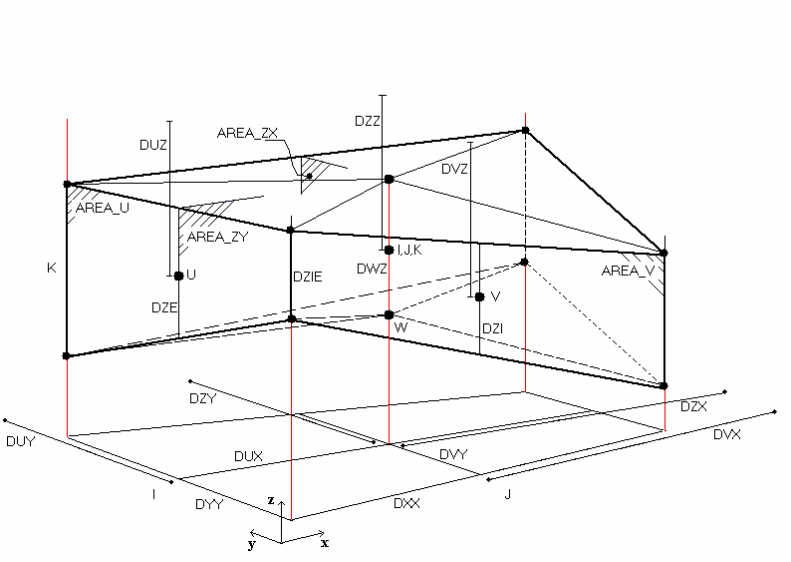

Figure 4-2: Finite volume element of MOHID model

4.3 Vertical Coordinates

Actually the module Geometry can divide the water column in different vertical coordinates: Sigma, Cartesian, Lagrangian (based on Sigma or based on Cartesian), “Fixed Spacing” and Harmonic. A subdivision of the water column into different domains is also possible. The Sigma and the Cartesian coordinates are the classical ones. The Cartesian coordinate can be used with or without “shaved cells”. The Lagrangian coordinate moves the upper and lower faces with the vertical flow velocity. The “Fixed Spacing” coordinate allows the user to study flows close to the bottom and the Harmonic coordinate works like the Cartesian coordinate, just that the horizontal faces close to the surface expand and collapse depending on the variation of the surface elevation. This coordinate was implemented in the geometry module to simulate reservoirs.

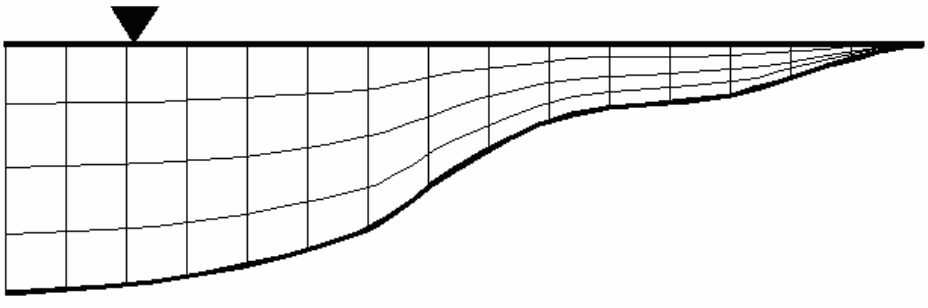

Figure 4-3: Sigma domain with 4 Layers

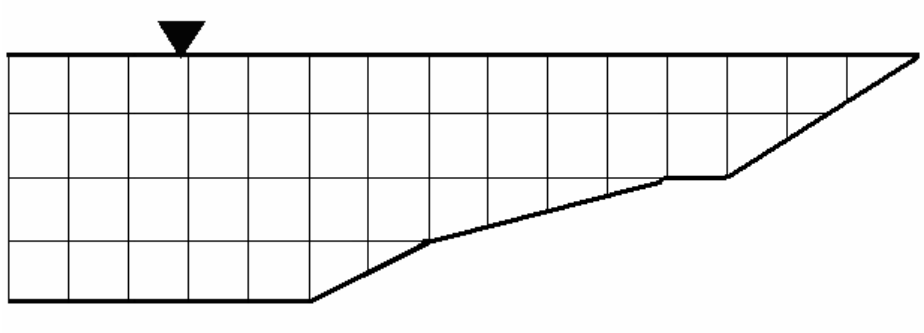

Figure 4-4: Cartesian domain with 4 Layers (shaved cells)

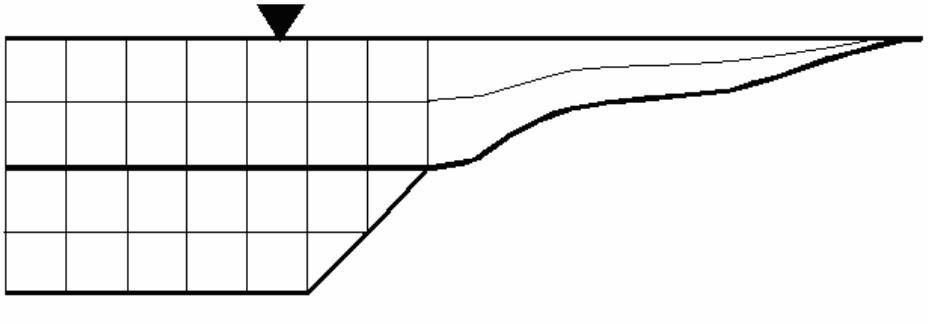

Figure 4-5: Sub-division of the water column in a Cartesian domain (inferior) and a Sigma domain (superior)

5 The Hydrodynamic Module

5.1 Introduction

In this section the hydrodynamic module of the model MOHID is described. The information flux of the hydrodynamic module, relative to the other modules of *Mohid*, is shown in Figure 5-1.

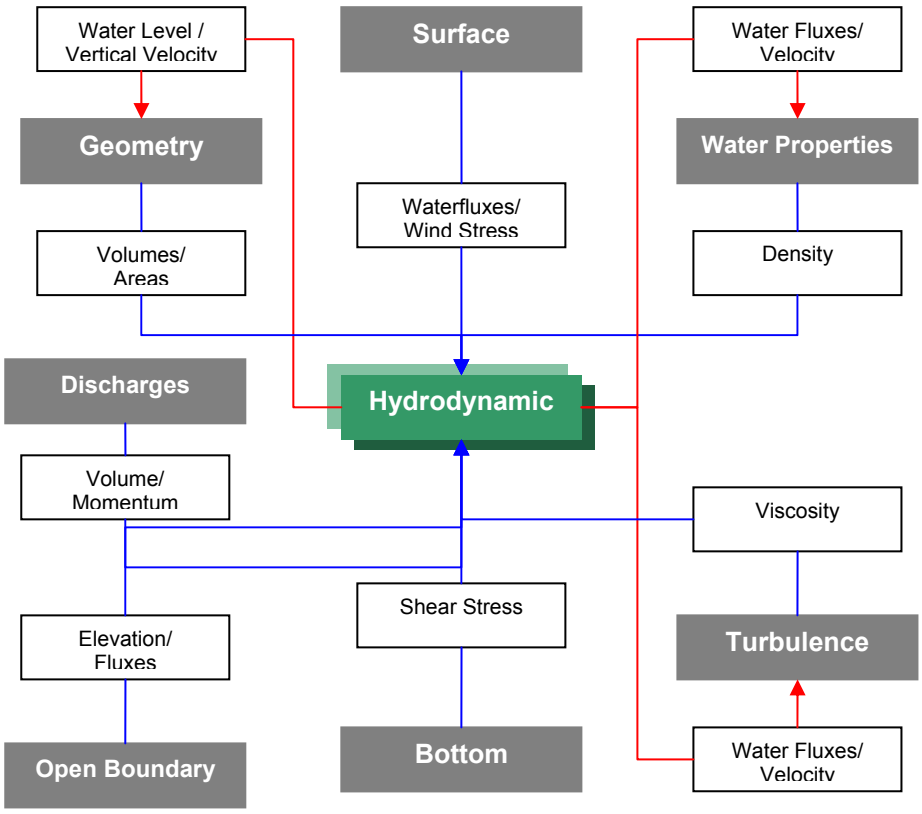

Figure 5-1: Information flux between the Hydrodynamic Module and other modules

5.2 Equations

The model solves the three-dimensional incompressible primitive equations. Hydrostatic equilibrium is assumed as well as Boussinesq and Reynolds approximations. All the equations below have been derived taken into account these approximations. The momentum balance equations for mean flow horizontal velocities are, in Cartesian form:

$$\partial_t u = -\partial_x(uu) - \partial_y(uv) - \partial_z(uw) + fv - \frac{1}{\rho_0}\partial_x p$$

$$+ \partial_x\left((\nu_H + \nu)\partial_x u\right) + \partial_y\left((\nu_H + \nu)\partial_y u\right) + \partial_z\left((\nu_t + \nu)\partial_z u\right) \qquad \text{Eq. 5-1}$$

$$\partial_t v = -\partial_x(vu) - \partial_y(vv) - \partial_z(uw) - fu - \frac{1}{\rho_0}\partial_y p$$

$$+ \partial_z\left((\nu_H + \nu)\partial_x v\right) + \partial_y\left((\nu_H + \nu)\partial_y v\right) + \partial_z\left((\nu_t + \nu)\partial_z v\right) \qquad \text{Eq. 5-2}$$

Where *u*, *v* and *w* are the components of the velocity vector in the x, y and z directions respectively, *f* the Coriolis parameter, ν_H and ν_t the turbulent viscosities in the horizontal and vertical directions, ν is the molecular kinematic viscosity (equal to 1.3 10^{-6} m^2 s^{-1}), *p* is the pressure. The temporal evolution of velocities (term on the left hand side) is the balance of advective transports (first three terms on the right hand side), Coriolis force (forth term), pressure gradient (next three terms) and turbulent diffusion (last three terms).

The vertical velocity is calculated from the incompressible continuity equation (mass balance equation):

$$\partial_x u + \partial_y v + \partial_z w = 0 \qquad \text{Eq. 5-3}$$

by integrating between bottom and the depth z where w is to be calculated:

$$w(z) = \partial_x \int_{-h}^{z} u dx + \partial_y \int_{-h}^{z} v dy \qquad \text{Eq. 5-4}$$

The free surface equation is obtained by integrating the equation of continuity over the whole water column (between the free surface elevation η(x,y) and the bottom -h):

$$\partial_t \eta = -\partial_x \int_{-h}^{\eta} u dz - \partial_y \int_{-h}^{\eta} v dz \qquad \text{Eq. 5-5}$$

The hydrostatic approximation is assumed with:

$$\partial_z p + g\rho = 0 \qquad \text{Eq. 5-6}$$

where g is gravity and ρ is density. If the atmospheric pressure p_{atm} is subtracted from p, and density ρ is divided into a constant reference density ρ_0 and a deviation ρ' from that constant reference density, after integrating from the free surface to the depth z where pressure is calculated, we arrive to:

$$p(z) = p_{atm} + g\rho_o(\eta - z) + g\int_z \eta\rho' dz \qquad \text{Eq. 5-7}$$

Eq. 5-7 relates pressure at any depth with the atmospheric pressure at the sea surface, the sea level and the anomalous pressure integrated between that level and the surface. By using this expression and the Boussinesq approximation, the horizontal pressure gradient in the direction x_i can be divided in three contributions:

$$\partial_{x_i} p = \partial_{x_i} p_{atm} - g\rho_0\partial_{x_i}\eta - g\int_z \eta\partial_{x_i}\rho' dz \qquad \text{Eq. 5-8}$$

The total pressure gradient is the sum of the gradients of atmospheric pressure, of sea surface elevation (barotropic pressure gradient) and of the density distribution (baroclinic pressure gradient). This decomposition of the pressure gradient is substituted in Eq. 5-1 and Eq. 5-2.

The density is obtained from the salinity and from the temperature, which are transported by the water properties module.

5.3 Discretization

5.3.1 Spatial discretization: Finite volume approach

The spatial discretization is described in the geometry module.

5.3.2 Temporal discretization: semi-implicit ADI algorithm

The temporal discretization is carried out by means of a semi implicit ADI (Alternate Direction Implicit) algorithm, introduced by Peaceman and Racford in 1955 (Fletcher, [1991]). This algorithm computes alternatively

one component of horizontal velocity implicitly while the other is calculated explicitly. The resulting equation system is a tridiagonal one that can be solved by Thomas algorithm in an efficient and quick way. This allows preserving the stability advantages of implicit methods without the drawbacks of computational expensiveness and associated phase errors. A longer time-step can therefore be used. Two different discretizations are coded in the model: a 4 equations one with two time levels per iteration- the S21 scheme (Eq. 5-9) by Abbott et al. [1973]- and the 6 equation algorithm by Leendertsee, [1967], more convenient when intertidal zones are to be modeled, since velocities are updated every half time step. The S21 scheme is shown by Eq. 5-9:

$$\eta^{t+1/2}(u^{t+1},u^{t},v^{t+1/2},v^{t-1/2}) \rightarrow u^{t+1} \rightarrow$$

$$w^{*t+1/2} \xrightarrow{GeometryUpdate} w^{t+1/2} \rightarrow S^{t+1/2},T^{t+1/2} \rightarrow$$

$$\eta^{t+1}(u^{t},u^{t+1},v^{t+3/2},v^{t+1/2}) \rightarrow u^{t+3/2} \rightarrow$$

$$w^{*t+1} \xrightarrow{GeometryUpdate} w^{t+1} \rightarrow S^{T+1},T^{T+1} \qquad \text{Eq. 5-9}$$

Each iteration is divided in two half steps. In the first half step, the free surface elevation η and then one of the horizontal velocities (u) are computed in an implicit way. The required value of the other velocity is taken from the previous time step. A vertical velocity w^* is computed from the continuity equation. Then, geometry is updated and the vertical velocity is corrected. The same process is followed in the next half step, but for the other component of horizontal velocity. In this diagram, salinity and temperature are computed each half step. As internal modes are much slower than external modes, S and T can be updated with a longer time step without losing accuracy and stability.

5.3.3 Discretization of the different processes

A sketch of the discretization will be given below. A full description of the discretization may be found in Martins, [2000] and Montero, [1999].

5.3.3.1 Free surface equation

Free surface elevation is calculated by integrating the continuity equation (Eq. 5-3) over the whole water column. In the finite volume approach, this integration is done via a summation the volume fluxes over all water column cells. For the S21 discretization and the first half time step, it reads:

$$\frac{\eta_{ij}^{t+1/2}-\eta_{ij}^{t}}{\Delta t/2}=$$

$$\frac{1}{A_{hij}}\left[\frac{1}{2}\left(\sum_{kbot}^{k\max}U_{ijk}^{t+1}A_{u_{ijk}}^{t}+\sum_{kbot}^{k\max}U_{ijk}^{t}A_{u_{ijk}}^{t}\right)-\frac{1}{2}\left(\sum_{kbot}^{k\max}U_{ij+1k}^{t+1}A_{u_{ij+1k}}^{t}+\sum_{kbot}^{k\max}U_{ij+1k}^{t}A_{u_{ij+1k}}^{t}\right)\right]$$

+

$$\frac{1}{A_{hij}}\left[\frac{1}{2}\left(\sum_{kbot}^{k\max}V_{ijk}^{t+1/2}A_{v_{ijk}}^{t}+\sum_{kbot}^{k\max}U_{ijk}^{t-1/2}A_{v_{ijk}}^{t}\right)-\frac{1}{2}\left(\sum_{kbot}^{k\max}V_{i+1jk}^{t+1/2}A_{u_{i+1jk}}^{t}+\sum_{kbot}^{k\max}U_{i+1jk}^{t-1/2}A_{u_{i+1jk}}^{t}\right)\right] \quad \text{Eq. 5-10}$$

where $A_{hij}=DUX_{ij}*DVY_{ij}$ is the area projected on the horizontal plane. Fluxes are temporally averaged, so the calculus is centered in t+1/2. An analogous discretization is carried out for the next half step. The fluxes $U\cdot AU$ and $V\cdot AV$ are obtained from the momentum equation. The discretization of the different terms will be discussed below.

5.3.3.2 Velocity equation

If we discretize equation (Eq. 5-1) making use of (**Error! Reference source not found.**) and S21 discretization, we arrive to (an equivalent equation is derived for *v*, Eq. 5-2) for every cell u_{ijk} of the grid:

$$\frac{\Omega_{u_{ijk}}^{t}(U_{ijk}^{t+1}-U_{ijk}^{t})}{\Delta t}+\sum_{m=1}^{Nfaces}\vec{F}\,\vec{n}\,A_m=f_{u_{ijk}}\Omega_{u_{ijk}}^{t}\overline{V}_{ijk}^{t} \quad \text{Eq. 5-11}$$

where $\Omega^{t}{}_{Uijk}$ is the volume of the computation cell for U_{ijk} and f_{uijk} is the value of the Coriolis parameter for that cell. The value $V,\overline{\ }^{t}{}_{ijk}$ represents the average value of the *v*-component of the flow on this cell. The second term on the left hand side represents the fluxes of the forces F_m through the surface A_m of the cell *m*. The Coriolis force is the term on the right hand

side and the other terms in the equation are included in the summation on the left hand side.

5.3.3.2.1 Coriolis term

As we can see on the right hand side of Eq. 5-11, the Coriolis term is discretized explicitly, although it is well-known that this implies a restriction on Δt ($\Delta t \leq 2/f$, with f the Coriolis parameter). This limitation is not critical for coastal applications -for latitude of 43º Δt ≤2000 s ≈ 5h 30min, that is much bigger than the time steps chosen in these applications.

The other terms in this formulation are seen as fluxes through the surfaces of the control volume, and therefore enter in the second term on the left hand side.

5.3.3.2.2 Advective terms

In order to guarantee momentum conservation, fluxes into the element must have null divergence. This is accomplished by using in the convective terms the same fluxes obtained in the last computation of elevation and vertical velocity. Convective fluxes are computed in every face of the cell:

$$-\sum_{m=1}^{Nfaces} \vec{F}_m \cdot \vec{n} A_m = \left[(U \cdot ufluxU)^t_{ij+1k} - (U \cdot ufluxU)^t_{ijk} + \right.$$

$$(U \cdot ufluxV)^t_{i+1jk} - (U \cdot ufluxV)^t_{ijk} +$$

$$\left. (U \cdot ufluxW)^t_{ijk+1} - (U \cdot ufluxW)^t_{ijk} \right] \qquad \text{Eq. 5-12}$$

with $ufluxU_i$ denotes the flux of U_i through the cell of calculus of u. A mixed scheme upwind-central differences is used for computing $ufluxU_i$ (James, [1987], Santos [1995]). Horizontal advective fluxes are discretized explicitly as the restriction that surface waves impose on stability is small for the characteristic range of velocities. The vertical advective term can give problems if the layer thickness is small, as can happen in shallow zones with sigma grids. Two solutions to this problem have been introduced in the model: an implicit discretization or neglecting this term in those regions.

5.3.3.2.3 Barotropic pressure gradient

The restriction of surface waves on stability lead to the implementation of the semi-implicit algorithm so this term limits stability and consequently is discretized implicitly. For the cell u_{ijk} and the first semi-step:

$$-\sum_{m=1}^{Nfaces} \vec{F}_m \cdot \vec{n} A_m = \frac{1}{\rho_0}\left[(P_{atm_{ij-1}}^{t+1/2} - P_{atm_{ij}}^{t+1/2}) + \rho_0 g(\eta_{ij-1}^{t+1/2} - \eta_{ij}^{t+1/2})\right] A_{u_{ijk}}^t \qquad \text{Eq. 5-13}$$

This expression, when substituted in the equation for the free surface, results in a tridiagonal system, which is solved by Gaussian elimination. In the equation for velocities, the values of η are already known, which allows the explicit discretization of this term for introduction in momentum equations.

5.3.3.2.4 Baroclinic pressure gradient

Internal modes do not introduce a stringent restriction on stability, so they can be discretized explicitly. The fluxes induced by this term through the faces of a uijk cell are:

$$-\sum_{m=1}^{Nfaces} \vec{F}_m \cdot \vec{n} S_m = \frac{g}{\rho_0}\left(\sum_{l=k+1}^{k\max}(\rho_{ij-1l}^{'t} DWZ_{ij-1l}) + \rho_{ij-1k}^{'t}\Delta z_{ij-1k}^t\right) A_{u_{ijk}}^t$$

$$-\left(\sum_{l=k+1}^{k\max}(\rho_{ijl}^{'t} DWZ_{ijl}) + \rho_{ijk}^{'t}\Delta z_{ijk}^t\right) A_{u_{ijk}}^t \qquad \text{Eq. 5-14}$$

where Δz_{ijk}^t represents the vertical distance from the cell top to the velocity point and arises as a consequence of the vertical staggering of the grid (ρ' is not defined in the same point as the u-velocity).

5.3.3.2.5 Horizontal diffusive fluxes

Horizontal diffusive fluxes are computed in every vertical face of the cell, applying that fluxes are normal to these faces:

$$-\sum_{m=1}^{Nfaces} \vec{F}_m \cdot \vec{n} A_m = (F_{ij-1/2k}^t Azx_{ij-1k}^t - F_{ij+1/2k}^t Azx_{ijk}^t) +$$

$$(F^t_{i-1/2\,jk}\frac{Av^t_{ijk}+Av^t_{ij-1k}}{2}-F^t_{i+1/2\,jk}\frac{Av^t_{i+1jk}+Av^t_{i+1j-1k}}{2}) \quad \text{Eq. 5-15}$$

Fluxes for x direction are:

$$F_{ij-1/2k}=\nu^t_{H_{ij-1k}}\frac{U^t_{ijk}-U^t_{ij-1k}}{DUX_{ij-1}} \quad \text{Eq. 5-16}$$

and for the y-direction:

$$F_{i-1/2\,jk}=\nu^t_{H_{i-1/2\,j-1/2k}}\frac{U^t_{ijk}-U^t_{ij-1k}}{\left(DYY_{ij}+DYY_{i-1j}\right)/2} \quad \text{Eq. 5-17}$$

where the horizontal viscosity coefficient ν^t_H is interpolated to the appropriate point.

5.3.3.2.6 Vertical diffusion

These terms must be discretized implicitly as the restriction imposed by an explicit discretization on the time step is strict for the resolution we will use.

$$-\sum_{m=1}^{Nfaces}\vec{F}_m\cdot\vec{n}\,A_m=(F^{t+1}_{ijk-1/2}-F^{t+1}_{ijk+1/2})A^t_{h_{ij-1/2}})+ \quad \text{Eq. 5-18}$$

with fluxes given by the equation:

$$F^{t+1}_{ijk-1/2}=\nu^t_{ij-1/2k-1}\frac{U^{t+1}_{ijk}-U^{t+1}_{ijk-1}}{DUZ^t_{ijk-1}} \quad \text{Eq. 5-19}$$

5.4 Boundary conditions

5.4.1 Free surface

All advective fluxes across the surface are assumed to be null. This condition is imposed by assuming that the vertical flux of *W* at the surface is null:

$$Wflux\Big|_{surface} = 0 \qquad \text{Eq. 5-20}$$

Diffusive flux of momentum is imposed explicitly by means of a wind surface stress, τ_w:

$$\nu \frac{\partial \overline{v_H}}{\partial z}\Big|_{surface} = \vec{\tau} w \qquad \text{Eq. 5-21}$$

Wind stress is calculated according to a quadratic friction law:

$$\vec{\tau w} = C_D \rho_a \vec{W} \left| \vec{W} \right| \qquad \text{Eq. 5-22}$$

where C_D is a drag coefficient that is function of the wind speed, ρ_a is air density and W is the wind speed at a height of 10 m over the sea surface.

5.4.2 Bottom boundary

Also at the bottom, advective fluxes are imposed as null and diffusive flux of momentum is estimated by means of a bottom stress that is calculated by a non-slip method with a quadratic law that depends on the near-bottom velocity. So, the diffusive term at the bottom is written as:

$$\nu \frac{\partial \vec{v}_H}{\partial z}\Big|_{bottom} = C_D \vec{v}_H \left| \vec{v}_H \right| \qquad \text{Eq. 5-23}$$

C_D is the bottom drag coefficient that is calculated with the expression:

$$C_D = \left(\frac{\kappa}{\log\left(\frac{z + z_0^b}{z_0^b} \right)} \right)^2 \qquad \text{Eq. 5-24}$$

where κ is von Karman constant and z^b_0 is the bottom roughness length. This quadratic law is derived from the logarithmic law of the wall near boundaries characteristic of boundary layers, as the bottom velocities are located half a grid box above the bottom. This term is calculated semi-implicitly following Backhaus [1985] for the sake of numerical stability.

No fluxes of salinity and temperature are considered at the bottom.

5.4.3 Lateral closed boundaries

At these boundaries, the domain is limited by land. For the resolution we are using, this lateral boundary layer is resolved, so a impermeable, free slip condition can be used:

$$\frac{\partial \vec{v}_H}{\partial \eta} = 0 \qquad \text{Eq. 5-25}$$

$$\vec{v} \cdot \vec{n} = 0 \qquad \text{Eq. 5-26}$$

In the finite volume formalism, these conditions are implemented straightforwardly by specifying zero normal water fluxes and zero momentum diffusive fluxes at the cell faces in contact with land.

5.4.4 Open boundaries

Open boundaries arise from the necessity of confining the domain to the region of study. The values of the variables must be introduced there such that it is guaranteed that information about what is happening outside the domain will enter the domain in a way that the solution inside the domain is not corrupted. Also, waves generated inside the domain should be allowed to go out. There exists no perfect open boundary condition and the most suitable would depend on the domain and the phenomena to be modeled. A recent review paper comparing open boundary conditions in test cases can be found in Palma and Matano [1999]. Some different open boundaries are already introduced in MOHID 3D (Santos, [1995], Montero, [1999]) and some others like FRS (Flow Relaxation Scheme) are in progress.

5.4.5 Moving boundaries

Moving boundaries are closed boundaries that change position in time. If there are inter tidal zones in the domain, some points can be alternatively covered or uncovered depending on tidal elevation. A stable algorithm is required for modeling these zones and their effect on hydrodynamics of

estuaries. A detailed exposition of the algorithms used in MOHID can be found in Martins et al. [1999] and Martins [1999].

6 The Lagrangian Module

6.1 Introduction

Lagrangian transport models are very useful to simulate localized processes with sharp gradients (submarine outfalls, sediment erosion due to dredging works, hydrodynamic calibration, oil dispersion, etc.).

Mohid's Lagrangian module uses the concept of tracer. The most important property of a tracer is its position (x,y,z). For a physicist a tracer can be a water mass, for a geologist it can be a sediment particle or a group of sediment particles and for a chemist it can be a molecule or a group of molecules. A biologist can spot phytoplankton cells in a tracer (at the bottom of the food chain) as well as a shark (at the top of the food chain), which means that a model of this kind can simulate a wide spectrum of processes.

The movement of the tracers can be influenced by the velocity field from the hydrodynamic module, by the wind from the surface module, by the spreading velocity from oil dispersion module and by random velocity.

At the present stage the model is able to simulate oil dispersion, water quality evolution and sediment transport. To simulate oil dispersion the lagrangian module interacts with the oil dispersion module, to simulate the water quality evolution the lagrangian module uses the feature of the water quality module. Sediment transport can be associated directly to the tracers using the concept of settling velocity.

Figure 6-1 represents the information flux between the lagrangian module and other modules of *Mohid*.

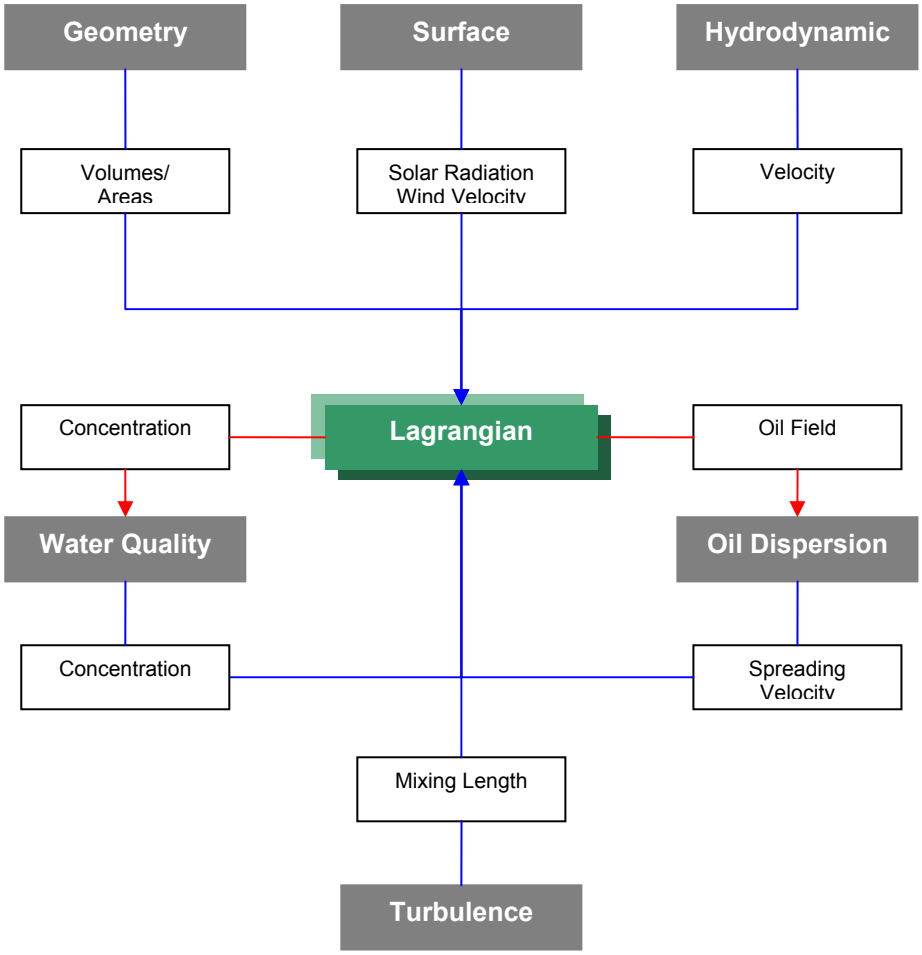

Figure 6-1: Information flux between the Lagrangian module and other modules

Another feature of the lagrangian transport model is the ability to calculate residence times. This can be very useful when studying the exchange of water masses in bays or estuaries.

6.2 Tracer concept

Like referred above, the *Mohid's* Lagrangian module uses the concept of tracer. The tracers are characterized by there spatial coordinates, volume and a list of properties (each with a given concentration). The properties can be the same one like the ones described in the water properties module or coliform bacteria. Each tracer has associated a time to perform the random movement.

The tracers are “born” at origins. Tracers which belong to the same origin have the same list of properties and use the same parameters for random walk, coliform decay, etc. Origins can differ in the way they emit tracers. There are three different ways to define origins in space:

- a “Point Origins” emits tracers at a given point;
- a “Box Origins” emits tracers over a given area;
- a “Accident Origins” emit tracers in a circular form around a point;

There are two different ways in which origins can emit tracers in time:

- a “Continuous Origins” emits tracers during a period of time;
- a “Instantaneous Origins” emits tracers at one instant;

Origins can be grouped together in Groups. Origins which belong to the same group are grouped together in the output file, so it is more easy to analyze the results.

6.3 Equations

6.3.1 Tracer Movement

The major factor responsible for particle movement is generally the mean velocity. The spatial co-ordinates are given by the definition of velocity:

$$\frac{dx_i}{dt} = u_i(x_i, t) \qquad \text{Eq. 6-1}$$

where *u* stands for the mean velocity and *x* for the particle position.

Equation 3.1 is solved using a simple explicit method:

$$x_i^{t+\Delta t} = x_i^t + \Delta t \cdot u_i^t \qquad \text{Eq. 6-2}$$

Higher order accuracy requires the use of an iterative procedure. The scheme adopted by Monteiro (1995) uses second order accuracy. Costa (1991) concluded that higher order schemes are important whenever curvature of the flow exists and a large time step is used. For most of the

natural flows the explicit method is accurate enough. Velocity at any point of space is calculated using a linear interpolation between the points of the hydrodynamic model grid. The lagrangian module permits to divide the calculation of the trajectory of the tracers into sub-steps of the hydrodynamic time step.

6.3.2 Turbulent Diffusion

Turbulent transport is responsible for dispersion. The effect of eddies over particles depends on the ratio between eddies and particle size. Eddies bigger than the particles make them move at random as explained in Figure 6-2. Eddies smaller than the particles cause entrainment of matter into the particle, increasing its volume and its mass according to the environment concentration, like shown in Figure 6-3.

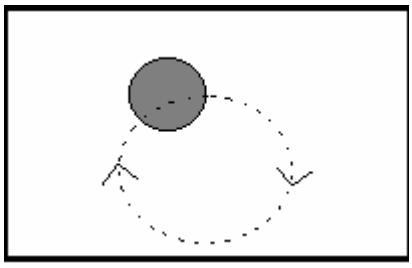

Figure 6-2: Random movement forced by an eddy larger than the particle

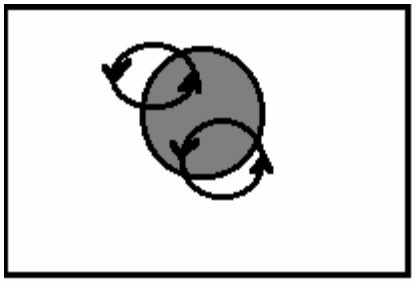

Figure 6-3: Random movement forced by an eddy larger than the particle

The random movement is calculated following the procedure of Allen (1982). The random displacement is calculated using the mixing length and the standard deviation of the turbulent velocity component, as given by the turbulence closure of the hydrodynamic model. Particles retain that velocity during the necessary time to perform the random movement, which is dependent on the local turbulent mixing length.

The increase in volume is associated with small-scale turbulence and is reasonable to assume it as isotropic. In these conditions, small particles keep their initial form and their increase in volume is a function of the volume itself.

6.3.3 Mass Decay rate

The decay rate of coliform bacteria, which are can associated to the tracers, is computed by the following equation:

$$\frac{dC}{dt} = -\frac{\ln 10}{T_{90}} C \qquad \text{Eq. 6-3}$$

where C represents the concentration, and T_{90} the time interval for 90% of the coliform bacteria to die.

An implicit method is used to solve Eq. 6-3 numerically, preventing a negative number of coliform bacteria.

6.3.4 Monitoring Boxes

The lagrangian module permits to monitor the distribution of particles inside “monitoring boxes”. This feature is very useful to compute the residence time of water inside these monitoring boxes and the origins of the water present inside each box at each moment. The lagrangian module “monitors” the boxes the following way:

- In every instant the volume of each box b, *InstBoxVol(b)* is calculated;

$$InstBoxVol(b) = \int (h + Z) dxdy$$

- In every instant the origin “o” of the water inside each monitoring box “b” is identified and the volume of the water from each origin is stored in the variable *InstVolumeByOrigin (b, o):*

$$InstVolumeByOrigin(b, o) = \sum_{o} Vol_j^b$$

- **In case of instantaneous emissions in boxes**, these contributions are integrated over the time, given the integrated contribution over the time, *IntgVolumeByOrigin(b, o)*

$$IntgVolumeByOrigin(b,o) = \int InstVolumeByOrigin(b,o)dt$$

A measure of the residence time of the water emitted into box “o” in monitoring box “b” is given by:

$$\mathrm{Re}\,sidenceTimePerBox(b,o) = IntgVolumeByOrigin(b,o) / IntialVol(o)$$

Adding the values for all monitoring boxes inside the estuary one gets the residence time inside the whole system of the water emitted into box “o”:

$$\mathrm{Re}\,sidenceTime(o) = \sum_{b} \mathrm{Re}\,sidenceTimePerBox(b,o)$$

These values also permit to compute how each monitoring box is influenced by each emitting box:

$$InfluenceOverBox(b,o) = IntgVolumeByOrigin(b,o) / InitialVol(b)$$

In case of a continuous emission, the residence time can be computed as:

$$\mathrm{Re}\,sidenceTimePerBox(b,o) = InstVolumeByOrigin(b,o) / Disch\,\mathrm{arg}\,eRate(o)$$

Again, the addition of the values of the residence time in each box gives the Residence time inside the System

- The Output is done in four ways:
    - Time Series in ASCII columns for every monitoring box and every time step. For every monitoring box a file is written where the first column represents the box volume and others represent the contributions to this box from every origin. Both, the instantaneous and the integrated values are written
    - Time Series in ASCII of the variable

ResidencetimeperBox(b,o)

- HDF Matrix for every Origin, every output instant. The relative contribution of each emitting box “o” for the instantaneous volume in each monitoring box “b” is written as the percentage of the instantaneous volume of the monitoring box:

Matrix(b,o) = 100 * *InstVolumeByOrigin(b,o) / InstBoxVol(b)*

HDF Matrix, one for all origins, every output time. The output Matrix is filled depending on the instantaneous contributions (in volume) of particle to a given monitor box. The missing volume is filled with 0 (freshwater).

7 The Oil Module

7.1 Introduction

The prediction and simulation of the trajectory and weathering of oil spills are essential to the development of pollution response and contingency plans, as well as to the evaluation of environmental impact assessments.

In order to predict the behaviour of the oil products spilled in coastal zones, an oil weathering model was developed, which predicts the evolution and behaviour of the processes (transport, spreading and behaviour) and properties of the oil product spilled in water. Some pollution response methods are also integrated in the model.

7.2 Implementation

Oil density and viscosity, and many different processes are included in oil module, such as oil spreading, evaporation, dispersion, sedimentation, dissolution, emulsification, oil beaching and removal techniques.

Different alternative methods were coded for the prediction of some processes like oil spreading, evaporation, dispersion, sedimentation and emulsification. Therefore, when using the model, there is more than one way of simulating the same process, depending, for example, on the characteristics of the computational mesh or on the magnitude of the spill.

The oil weathering module (OWM) uses mainly the 3D hydrodynamics and 3D lagrangian transport modules. The hydrodynamic module simulates the velocity field necessary for the lagrangian module to calculate oil trajectories. These oil trajectories are computed assuming that oil can be idealized as a large number of particles that independently move in water. Water properties and atmospheric conditions are introduced in lagrangian module and used by oil module for determination of oil processes and properties. Excepting spreading and oil-beaching, all weathering processes and properties are assumed uniform for all tracers, like water properties and atmospheric conditions, which are considered equal to these environmental conditions determined in accident origin.

As it was already mentioned, the movement of the oil tracers can be influenced by the velocity field from the hydrodynamic module, by the wind from the surface module, by the spreading velocity from oil module and by random velocity.

Oil temperature is assumed equal to water temperature, neglecting solar radiation or any other energy transfer process that may influence oil temperature.

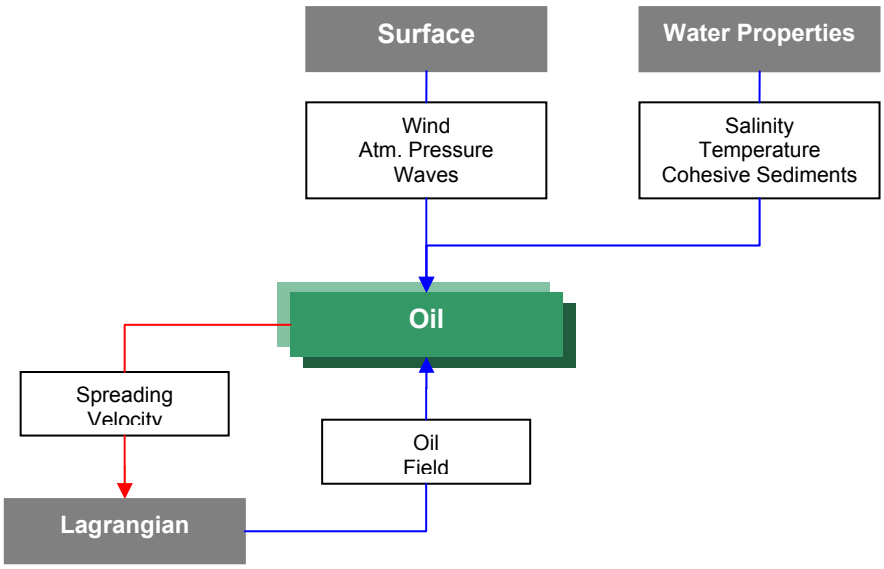

Figure 7-1 Information flux between the oil module and other modules

7.3 Equations

7.3.1 Spreading

In case of an instant accident, the initial area of spilled oil is determinated by an equation deduced from Fay's solutions (Fay, 1969). Once initial phase of spreading (gravity-inertial phase) is too short, initial area is calculated when that phase ends, and gravity-viscous phase starts:

$$A_0 = \pi \frac{k_2^4}{k_1^2} \left(\frac{\Delta g V_0^5}{\nu_w} \right)^{1/6} \qquad \text{Eq. 7-1}$$

Where:

A_0 – initial area

$\Delta = (\rho_w - \rho_o)/\rho_w$

ρ_w– water density

ρ_o- oil density

g – gravity acceleration

V_0 – volume of spilled oil

ν_w– water kinematic viscosity

k_1 = 0.57 and k_2=0.725 (as recommended by Flores et al 1999)

Two different algorithms were implemented to estimate oil spreading.

One of the algorithms determines random velocities u_d e v_d (with uniform distribution) inside range [$-U_r$, U_r], [$-V_r$,V_r] (in directions x and y, respectively) proportional to diffusion coefficients, which are calculated assuming that lagrangian tracers spreading is equivalent to Fay's formulas solution (Fay, 1969). The following relationship between diffusion coefficients D_x and D_y and the velocity fluctuation range [$-U_r$, U_r], [$-V_r$,V_r] is adopted according to Leitão (1996):

$$U_r = \sqrt{\frac{2D_x}{\Delta t}} \qquad \text{Eq. 7-2}$$

$$V_r = \sqrt{\frac{2D_y}{\Delta t}} \qquad \text{Eq. 7-3}$$

Random velocities are therefore determined in the following way, like suggested by Proctor *et al.*(1994):

$$u_d = R_1 \cos(2\pi R_2) \cdot U_r \qquad \text{Eq. 7-4}$$

$$v_d = R_1 sen(2\pi R_2) \cdot V_r \qquad \text{Eq. 7-5}$$

where R_1 e R_2 are randomly generated numbers between 0 and 1.

The only phase simulated in spreading is the gravity-viscous phase, from solutions proposed by Fay, where diffusion coefficients D_x and D_y have the following formulation(this model uses a numerical solution of this equation):

$$D_x = D_y = \frac{\pi k_2^2}{16}\left(\frac{\Delta g V^2}{v_w^{1/2}}\right)^{1/3} \cdot \frac{1}{\sqrt{t}} \qquad \text{Eq. 7-6}$$

Where:

V- volume of spilled oil

t – time after spill

The other algorithm proposed for oil spreading is based in thickness differences inside oil slick, presuming that the existence of a thickness gradient generates a “spreading force” in the direction of minor thickness. Therefore, a tracer will move from the computational cell with larger oil thickness to the one thinner.

This formulation uses a coefficient to approach the solution to the Fay solution, in order to make results sensible to some factors, like different oil densities, originating different behaviours.

Spreading coefficient is given by:

$$k = k_1 \cdot \frac{\Delta^{1,6} g V^2}{v_w^{1/6}} \qquad \text{Eq. 7-7}$$

where k_1 is a parameter introduced by the user, with a default value of 10.0.

Therefore, in oil module velocities are calculated in the faces of cells where oil is present, in directions *x* and *y*, in the following way:

$$u_{cell} = k \cdot \frac{\Delta h}{\Delta x} \qquad \text{Eq. 7-8}$$

$$v_{cell} = k \cdot \frac{\Delta h}{\Delta y} \qquad \text{Eq. 7-9}$$

where $\frac{\Delta h}{\Delta x}$ and $\frac{\Delta h}{\Delta y}$ are the thickness gradients of a cell, in directions *x* and *y*. Subsequently, in lagrangian module tracers velocities are interpolated based on cell faces velocities and tracers position.

If average oil thickness becomes too thin – less than a value between 0.1 and 0.01 mm, depending of product viscosity –, oil spreading is stopped, according to Reed (1989).

7.3.2 Density

Density can be estimated by:

$$\rho_e = F_{wv} \cdot \rho_w + \rho_{oil}(1 - F_{wv})(1 + c_{DE}F_e)\left[1 - c_{DT}(T - T_0)\right] \qquad \text{Eq. 7-10}$$

where ρ_e is the density of the emulsion at temperature T, ρ_{oil} is the density of fresh oil at reference temperature T_0 , ρ_w is the water density, c_{DE} e c_{DT} are empirical constants (NOAA (1994) recommends the following values: c_{DE} = 0.18 and c_{DT} = 8x10^{-4}).

The oil initial density is obtained from API density. Only oil products with lower density than water are modelled, because the remainder will sink.

7.3.3 Viscosity

Viscosity is changed by three major processes: temperature, evaporation and emulsification.

The influence of temperature can be calculated by Andrade's correlation:

$$\mu = \mu_0 e^{c_T\left(1/T - 1/T_0\right)} \qquad \text{Eq. 7-11}$$

where μ is the oil viscosity at temperature T, μ_0 is the initial oil viscosity at reference temperature T_0 and c_T is an empirical constant whose recommended value by NOAA (1994) is 5000 K.

Viscosity modification due to emulsification is defined by Mooney's equation (1951):

$$\mu = \mu_0 e^{\left[\frac{c_V F_{wv}}{(1-c_M F_{wv})}\right]} \qquad \text{Eq. 7-12}$$

where F_{wv} is water volume fraction the emulsion, c_V is an adimensional empirical constant (Mackay et al., 1980 recommends the value of 2.5) and c_M is an additional Mooney's constant with the value of 0.65.

The effect of evaporation on viscosity is calculated by the following equation (Mackay et al., 1980):

$$\mu = \mu_0 \cdot e^{(c_E F_{em})} \qquad \text{Eq. 7-13}$$

F_{em} is the mass fraction of evaporated oil, and the adimensional empirical constant c_E varies with oil type, between 1 and 10, with higher values for more viscous products. In this model, when fresh oils at 15ºC have a cinematic viscosity greater than 38 cSt, c_E is always considered 10. In case of less viscous oils, c_E is estimated by a second degree polynomial regression:

$$c_E = -0.0059 \cdot V_{cin15}^2 + 0.4461 \cdot V_{cin15} + 1.413 \qquad \text{Eq. 7-14}$$

where V_{cin15} is the oil cinematic viscosity at 15ºC.

The three previous equations (Eq. 7-11, Eq. 7-12 and Eq. 7-13) can be joined in a single equation:

$$\mu = \mu_0 \cdot e^{\left[(c_E F_{em}) + \frac{c_V F_{wv}}{(1-c_M F_{wv})} + c_T\left(1/T - 1/T_0\right)\right]} \qquad \text{Eq. 7-15}$$

7.3.4 Evaporation

In MOHID, the oil evaporation process can be estimated by two different methods: an analytical method, also known as the evaporative exposure method (developed by Stiver & Mackay, 1984), and by a more recent methodology proposed by Fingas (1998).

Evaporative exposure method is given by the formula:

$$\frac{dF_e}{dt} = \frac{K_e A_s}{V_0} \cdot \exp\left(A - \frac{B}{T}(T_0 + T_G F_e) \right) \quad \text{Eq. 7-16}$$

F_e is the volume fraction of evaporated oil, T is oil temperature, A_s is the oil slick area, V_0 is the initial oil volume, K_e is the mass transfer coefficient, determined by a simple formulation proposed by Buchanan & Hurford (1988):

$$K_e = 2.5 \times 10^{-3} W^{0.78} \quad \text{Eq. 7-17}$$

A and B are empirical constants, T_o is the initial boiling point and T_G is the distillation curve gradient. All these parameters depend of oil type. In this model, they are estimated, and T_o e T_G are obtained from *API* density, according to version 1.1 of ADIOS model (NOAA, 1994):

A = 6.3; B = 10.3

For crude oils:

$$T_0 = 532.98 - 3.1295 \cdot API \quad \text{Eq. 7-18}$$

$$T_G = 985.62 - 13.597 \cdot API \quad \text{Eq. 7-19}$$

For refined products:

$$T_0 = 654.45 - 4.6588 \cdot API \quad \text{Eq. 7-20}$$

$$T_G = 388.19 - 3.8725 \cdot API \quad \text{Eq. 7-21}$$

Mervin Fingas proposed other method for evaporation calculus. He proposed a simplified formulation, where the relevant factors are time and temperature.

For many oil types, Fingas determined specific empirical equations in the following forms (this model uses the numerical solutions of the following equations):

$$\%Ev = (\alpha + \beta \cdot T)\ln(t) \qquad \text{Eq. 7-22}$$

or

$$\%Ev = (\alpha + \beta \cdot T)\sqrt{t} \qquad \text{Eq. 7-23}$$

where *%Ev* is the percentage (by weight) of evaporated oil, *α* and *β* are empirical constants specific for each oil type, *T* is oil temperature, *t* is time after spill (minutes).

If empirical data is unknown, generically equations can be used:

$$\%Ev = \left[(0.165(\%D) + 0.045 \cdot (T - 15)\right]\ln(t) \qquad \text{Eq. 7-24}$$

or

$$\%Ev = \left[(0.0254(\%D) + 0.01 \cdot (T - 15)\right]\sqrt{t} \qquad \text{Eq. 7-25}$$

%D is the percentage (by weight) distilled at 180ºC.

Square root equations are used in some refined oils and in short term simulations (1-2 days).

7.3.5 Emulsification

This process consists in incorporation of water in oil. This process usually starts after an amount of oil has evaporated. An emulsification constant is used, which means the percentage of oil evaporated before emulsification starts. By default, this constant is 0%.

When emulsification starts, incorporation of water in oil can be simulated by two different processes.

An equation widely used, proposed by Mackay *et al.* (1980), is implemented in this model:

$$\frac{dF_{wv}}{dt} = K_w\left(1+W\right)^2\left(1-\frac{F_{wv}}{F_{wv}^{final}}\right) \quad \text{Eq. 7-26}$$

where F_{wv} is the water volume fraction incorporated in emulsion; F_{wv}^{final} is the final volume fraction of water incorporated in emulsion; K_w is an empirical constant, introduced by the model user. Usually this constant assume values between 1.0×10^{-6} and 2.0×10^{-6}. MOHID default value is 1.6×10^{-6}, which is also used in ADIOS model (NOAA, 1994).

The other algorithm used is Rasmussen equation (Rasmussen, 1985).

$$\frac{dF_{wv}}{dt} = R_1 - R_2 \quad \text{Eq. 7-27}$$

where:

R_1 - water incoming rate (s^{-1}), given by:

$$R_1 = \frac{K_1}{\mu_0}\left(1+W\right)^2\left(F_{wv}^{final} - F_{wv}\right) \quad \text{Eq. 7-28}$$

R_2 - water outgoing rate (s^{-1}), given by:

$$R_2 = \frac{K_2}{Asph\cdot Wax\cdot\mu_0}F_{wv} \quad \text{Eq. 7-29}$$

Asph is the asphaltene content in oil (%), *Wax* is the wax content (%), and K_1 e K_2 are experimentally determined constants by Rasmussen (1985):

K_1 = 5x10^{-7} kg.m^{-3} ; K_2 = 1.2x10-7 kg.m^{-1}.s^{-2}.

7.3.6 Dispersion

This is the process where oil droplets entrain in water column.

Two different methods are available to predict this weathering process. One of them is Delvigne & Sweeney (1988) method:

$$\frac{dm_d}{dt} = c_{oil} \cdot D_{ba}^{0,57} \cdot f_s \cdot F_{wc} \cdot d_0^{0,7} \cdot \Delta d \qquad \text{Eq. 7-30}$$

This equation estimates mass transfer rate per time unit, where f_s is the surface fraction covered by oil (considered equal to oil content in emulsion water + oil); d_0 is the droplet diameter; Δd is the oil droplets diameters range around d_0 (model assumes a droplet size range between 5 – 70 microns. Bigger droplets will tend to resurface - NOAA, 1994); c_{oil} is a parameter experimentally determined which depends on oil type. This model uses a logarithmical regression based on oil cinematic viscosity:

$$c_{oil} = -312.25 \cdot \ln(V_{cin}) + 2509.8 \qquad \text{Eq. 7-31}$$

where V_{cin} is the oil cinematic viscosity

(if this regression gives negative values, c_{oil} is considered 0)

D_{ba} is the wave dissipation energy per unit of surface area, which can be calculated by:

$$D_{ba} = 0.0034 \rho_w g H_{rms}^2 \qquad \text{Eq. 7-32}$$

H_{rms} is:

$$H_{rms} = \frac{1}{\sqrt{2}} H_0 \qquad \text{Eq. 7-33}$$

where H_0 is wave height.

F_{wc} is the fraction of the sea surface that is covered with whitecaps per time unit, given by:

$$F_{wc} = \frac{C_b (W - W_i)}{T_w} \qquad \text{Eq. 7-34}$$

where C_b =0,032 s.m^{-1} , W_i is the wind velocity to start whitecaps (4 m.s^{-1}); T_w is the wave period.

If wave period and wave height are unknown, these properties can be

empirically determined as function of wind speed, according to ADIOS model formulations (NOAA, 1994):

$$H_0 = 0.243\frac{W^2}{g} \qquad \text{Eq. 7-35}$$

and

$$T_w = 8.13\frac{W}{g} \qquad \text{Eq. 7-36}$$

Once turbulent energy is difficult to determine, other simplified algorithms have been developed for vertical dispersion in function of square wind velocity. One of them is used in this model – the formulation proposed by Mackay *et al.* (1980):

$$\frac{dm_d}{dt} = 0.11 m_{oil}\frac{(1+W)^2}{1+50\mu^{1/2}h\sigma} \qquad (\text{kg.h}^{-1}) \qquad \text{Eq. 7-37}$$

, where m_{oil} is the oil mass that remains in surface, μ is the oil dynamic viscosity (cP), h is the slick thickness (cm), W is the wind velocity(m.s^1) and σ is oil-water interfacial tension (dyne.cm^{-1}).

7.3.7 Sedimentation

Although oil sedimentation process is relatively complicated and difficult to estimate, a formulation developed by Science Applications International (Payne *et al.*, 1987) is used in MOHID:

$$\frac{dm_{sed}}{dt} = 1.3\sqrt{\frac{E}{V_w}}K_a \cdot C_{oil} \cdot C_{sed} \cdot z_i \cdot A_s \qquad \text{Eq. 7-38}$$

This equation gives the mass of sedimented oil per time unit (kg.s^{-1}), where:

Vw is the water dynamic viscosity (kg.m^{-1}.s^{-1}); Ka is the stick parameter with value 1×10^{-4} m^3.kg^{-1}; z_i is the intrusion depth of oil droplets in the water column due to breaking waves, given by Delvigne & Sweeney (1988):

$$z_i = 1.5 \cdot H_0 \qquad \text{Eq. 7-39}$$

E is the rate of dissipated energy from water surface (J.m^{-3}.s-1). This is estimated from the wave dissipation energy (D_{ba}), previously explained in dispersion section:

$$E = \frac{D_{ba}}{z_i \cdot T_w} \qquad \text{Eq. 7-40}$$

C_{sed} is the sediment concentration in water column (kg.m^{-3}), C_{oil} is the oil droplet concentration in water column (kg.m^{-3}). This concentration can be determined from dispersion rate proposed by Delvigne & Sweeney (1988) (explained in dispersion section), integrating this rate for wave period and intrusion depth of oil droplets:

$$\frac{dC_{oil}}{dt} = \frac{\frac{dm_d}{dt}}{z_i} \qquad \text{Eq. 7-41}$$

Only droplets greater than 70 microns and smaller than 200 microns are considered for sedimentation. Bigger droplets are less probable to stick to sedimented particulate matter, and smaller than 70 microns are already estimated in dispersion process.

7.3.8 Dissolution

This process may be quantified through Cohen method, where dissolution rate is estimated by:

$$\frac{dDiss}{dt} = K \cdot f_s \cdot A_s \cdot S \qquad (\text{g.h}^{-1}) \qquad \text{Eq. 7-42}$$

f_s is the surface fraction covered by oil (considered equal to oil content in emulsion water + oil); A_s is the oil slick area (m^2) and *S* is the oil solubility in water. Huang & Monastero (1982) proposed an analytical solution for the solubility of a typical oil (this model uses the numerical solutions of the following equation):

$$S = S_0 \cdot e^{\alpha t} \qquad \text{Eq. 7-43}$$

where S_0 s the solubility of the "fresh" oil (30 g.m^3); α is a decayment constant (0.1); t is the time after spill (h) and K is the dissolution mass transfer coefficient (0.01m.h^{-1})

7.3.9 Oil-Beaching

When oil reaches a coastal zone, it might become beached. This model estimates the amount of beached oil when the model user predefines a beaching probability (or different beaching probabilities for different coastal zones).

7.3.10 Removal techniques

Some removal techniques like chemical dispersion or mechanical cleanup are also included in model.

7.3.10.1 *Chemical Dispersion*

The application of chemical dispersants is simulated since dispersant efficiency, percentage of oil slick sprayed, and application period are known. The chemical dispersed rate is predicted by the following equation:

$$\frac{dm_{Qchem}}{dt} = \frac{m_{oil} \cdot \left(\frac{\%A_{spr}}{100}\right) \cdot \left(\frac{\%Ef}{100}\right)}{\Delta t} \qquad \text{Eq. 7-44}$$

m_{oil} is the instant mass of oil $\%A_{spr}$ is the percentage of total slick area sprayed by the chemical dispersant, and $\%Ef$ is the efficiency of the chemical product.

7.3.10.2 *Mechanical Cleanup*

Mechanical Cleanup is also simulated for a certain time period, where the volume rate or total emulsion removed during that period must be known.

If emulsion volume rate removed by the skimmer is unknown, it is obtained from the total volume of emulsion mechanically removed in the operation

time period:

$$\frac{dV_{mec}}{dt} = \frac{\frac{V_{TotMec}}{1000}}{\Delta t} \qquad \text{Eq. 7-45}$$

Where V_{TotMec} is the total volume of emulsion mechanically removed (m^3/h) and $\frac{dV_{mec}}{dt}$ is the volume rate of emulsion mechanically removed (l/h).

After a conversion of this emulsion volume rate to m^3/s , the rate of oil volume removed is estimated by:

$$\frac{dV_{OilMec}}{dt} = \frac{dV_{mec}}{dt} \cdot (1 - Y) \qquad \text{Eq. 7-46}$$

Where Y is the water content in emulsion water + oil.

8 The Water Properties Module

8.1 Introduction

The water properties module coordinates the evolution of the water properties in the water column, using a eulerian approach. This coordination includes the transport due advective and diffuse fluxes, water discharges from rivers or anthropogenic sources, exchange with the bottom (sediment fluxes) and the surface (heat fluxes and oxygen fluxes), sedimentation of particulated matter and the internal sinks and sources (water quality).

Actually the model *Mohid* can simulate 24 different water properties: temperature, salinity, phytoplankton, zooplankton, particulate organic phosphorus, refractory dissolved organic phosphorus, non-refractory dissolved organic phosphorus, inorganic phosphorus, particulate organic nitrogen, refractory organic nitrogen, non-refractory organic nitrogen, ammonia, nitrate, nitrite, biological oxygen demand, oxygen, cohesive sediments, ciliate bacteria, particulate arsenic, dissolved arsenic, larvae and fecal coli-forms. Any new property can be added very easily, due to the object orientated programming used within the *Mohid* model.

In the water quality module, the nitrogen, oxygen and phosphorus cycle can simulate the terms of sink and sources. Figure 8-1 represents the information flux of the water properties module.

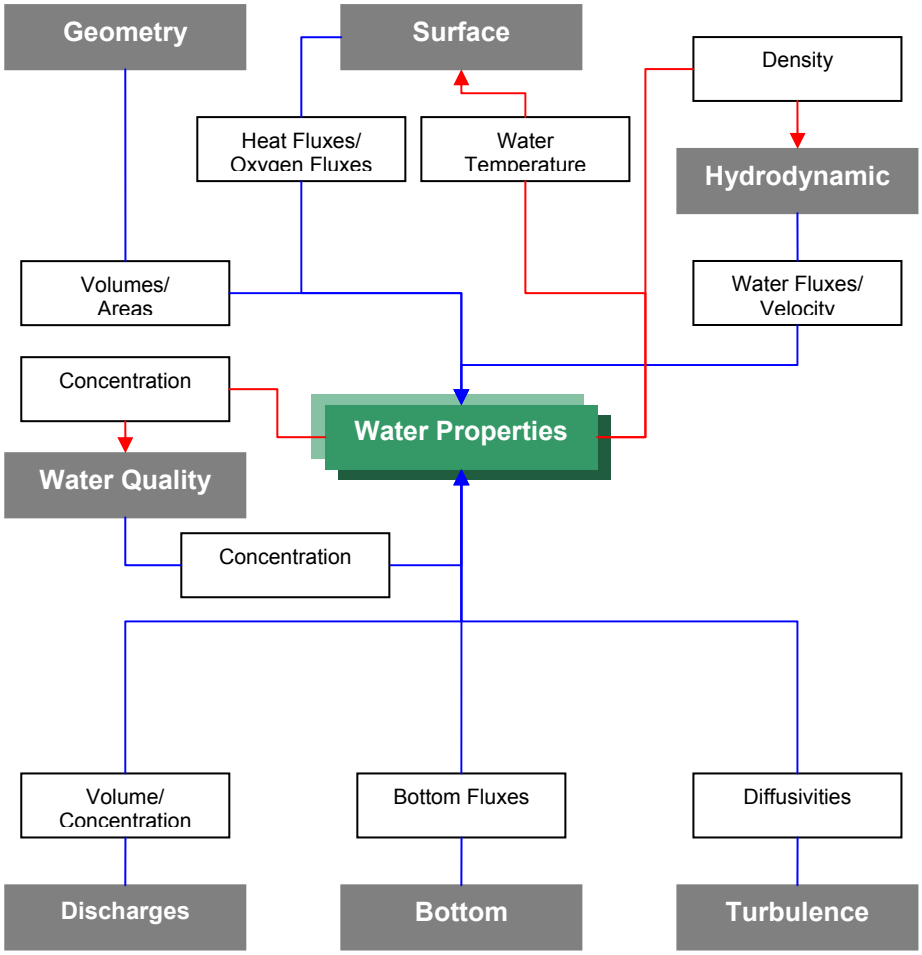

Figure 8-1: Information flux between the Water Properties Module and other modules

8.2 Equations

8.2.1 Transport

The transport due advective and diffusive fluxes, of a given property *A*, is resolved by the following equation:

$$\partial_t A = -\partial_x(uA) - \partial_y(vA) - \partial_z(wA)$$

$$+\partial_x(\nu'_H\,\partial_x A) + \partial_y(\nu'_H\,\partial_y A) + \partial_z\left((\nu'_t + \nu'_A)\partial_z A\right) \qquad \text{Eq. 8-1}$$

where *u*, *v* and *w* are the velocity in x, z and z direction, ν'_H and ν'_t the horizontal and vertical eddy diffusivities, and ν'_A the molecular diffusivity.

The temporal evolution of A is the balance of advective transport by the mean flow and turbulent mixing and the possible sink and sources the property may have.

8.2.2 Density

The density ρ is calculated as a function of temperature and salinity by a simplified equation of state (*Leendertsee and Liu, [1978]*):

$$\rho = (5890 + 38T - 0.375T^2 + 3S) /$$

$$((1779.5 + 11.25T - 0.0745T^2) - (3.8 + 0.01T)S +$$

$$0.698(5890 + 38T - 0.375T^2 + 3S)) \qquad \text{Eq. 8-2}$$

That is an approximation for shallow water of the most widely used UNESCO equation (UNESCO, [1981]).

9 The Water Quality Module

9.1 Introduction

Today, efforts towards ecological modeling are being made in most countries were water quality management is a major concern. Fransz *et al.*, (1991) notice that most new generation models tend to become much more biologically and chemically diversified than earlier models, as it is now largely recognized that there is no way to simulate in sufficient detail the ecosystem behavior without an in-depth treatment of the full cycle of organic matter.

These processes are not foreign to the preoccupations caused by the eutrophication and its various manifestations. Although there is general consensus that the inputs of nutrients to the sea must be reduced there is so far no firm scientific basis to decide upon the extent of such reductions.

An appropriate way of addressing the problem of eutrophication and of testing nutrient reduction scenarios is to simulate the phenomenon with mathematical models. It is probably correct to assume that any ecological model with a sufficiently complex internal structure and the multiple relationships that are found at the lower trophic levels will come close to an answer, provided the right time scale is applied.

The ecological model included in *Mohid* is adapted from EPA, (1985) and pertain to the category of ecosystem simulations models i.e. sets of conservation equations describing as adequately as possible the working and the interrelationships of real ecosystem components. It's not correct to say that the model describes the lower trophic levels with great accuracy. In fact the microbial loop that plays a determinant role in water systems in the recycling processes of organic waste is very simplified in our model.

Lower trophic levels appear in nearly all marine ecosystem simulation models since there is at least a compartment "phytoplankton" required to drive the organic matter cycle. Some early models applied in the North Sea were one-compartment models, especially endeavouring to simulate phytoplankton growth, in relation with the physical environment and with

grazing pressure (treated as a forcing variable). Both the influence of the Lotka-Volterra equations – developed in the 1920s – and that of findings in the field of plant physiology (photosynthesis-light relationship) were discernible. It was not long before limiting nutrient and herbivorous zooplankton were incorporated as well, as state variables in simulation models. (Fransz *et al.*, 1991)

9.2 The general model

Franz *et al.* (1991) defined the general conservation equations for an idealized marine ecosystem model. Here we have adapted their definitions and establish a system that consists in five general state variables including phytoplankton, zooplankton, dissolved nutrient, organic matter in pelagic phase, organic matter in benthic phase, pelagic bacteria, benthic bacteria.

---

dN/dt = $- f_{12}$ (uptake by phytoplankton) – f_{15} (uptake by pelagic bacteria) + f_{51} (pelagic mineralization) + f_{61} (benthic mineralization) + f_{01} (excretion by zooplankton) + advection and diffusion

dP/dt = $+f_{12}$ (phytoplankton growth)) – f_{23} (excretion of pOM) – (f'_{23} + f'_{24}) (natural mortality) – f_{20}(grazing) – f_{24} (phytoplankton sinking) + advection and diffusion.

dZ/dt = + f_{20} (zooplankton growth) – f_{01} (excretion of nutrients) – f_{04} (excretion of bOM) - f_{03} (excretion of pOM)

dpOM/dt = $+f_{23}$ (excretion of pOM) + f'_{23} ((1-a).natural mortality of phytoplankton) + f_{53} ((1-b).natural mortality of pelagic bacteria) + f_{03} ((1-c).feacal pellets and detritus from upper trophic levels) – f_{35} (pOM degradation by pelagic bacteria) + advection and diffusion.

dbOM/dt = $+f'_{24}$ ((a).natural mortality of phytoplankton) + f_{24} (phytoplankton sinking) $+f_{54}$ ((b). natural mortality of pelagic bacteria) + f_{64} (natural mortality of benthic bacteria) + f_{04} ((c).feacal pellets and detritus from upper trophic levels) – f_{46} (bOM degradation by benthic bacteria) + advection and diffusion.

dpB/dt = $+f_{35}$ (pOM degradation) + f_{15} (N uptake) – f_{51} (pelagic mineralization) – (f_{53} + f_{54}) (natural mortality) + advection and diffusion.

dpB/dt = $+f_{46}$ (bOM degradation) – f_{61} (benthic mineralization) $-f_{64}$ (natural mortality).

where *N* represents the concentration of dissolved inorganic nutrient, *P* the concentration of concentration of phytoplankton, *Z* the concentration of zooplankton, *pOM* theconcentration of pelagic organic matter, *bOM* the concentration of benthic organic matter, *pB* the concentration of pelagic bacteria, *bB* the concentration of benthic bacteria and *a, b, c* factors comprised between 0 and 1.

The primary production process, powered by light energy, is the necessary engine for all transfers of mass between biological compartments. Zooplankton that on early days was not explicitly modeled it's now considered an important state variable.

The *Mohid* Water Quality module is a zero-dimensional ecological model, which can be used by the eulerian or the lagrangian transport modules. The nitrogen cycle, oxygen cycle and the phosphorus cycle are included. A brief description of these cycles is presented in the next sections. Figure 9-1 represents the information flux between the water quality module and other modules.

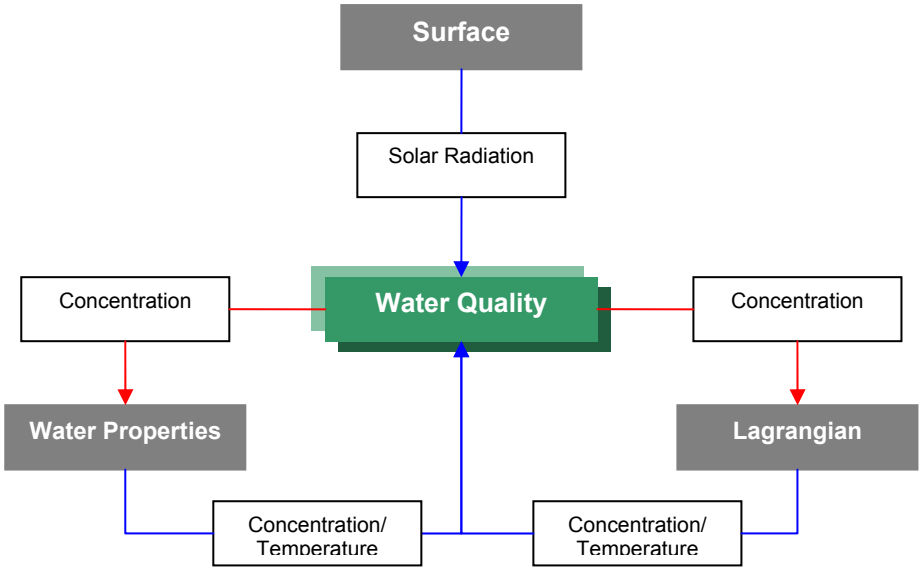

Figure 9-1: Information flux between the water quality module and other modules

The water quality module has been developed in terms of sinks and sources. Such an approach is convenient to give these models the desired flexibility. Because of the properties interdependency a linear equation system is computed for each control volume and this system can be compute forward or backward in time.

Many of the equations described in the next sections are written as dependent on a regulating factor, which contains the functional response of the organism to some environmental parameters such as light, nutrients or temperature. When growth is a function of many resources, there is a large range of functional forms that might express the joint dependence. To control the various possibilities, it is common to think of separate resources as limiting factors reducing some theoretical maximum growth rate - factors that can be determined separately and the combined by a small number of ways.

Each growth limitation factor can range from a value of 0 to 1. A value of 1 means the factor does not limit growth (i.e. is at optimum intensity, nutrients are available in excess, etc) and a value of 0 means the factor is so severely limiting that growth is inhibit entirely.

Four major approaches have been used to combine the limiting factors:

- A multiplicative formulation in which all factors are multiplied together. This approach assumes that several nutrients in short supply will more severely limit growth than a single nutrient in short supply. The major criticism of this approach is that the computed growth rates may be excessively low when several nutrients are limiting. Also, the severity of the reduction increases with the number of limiting nutrients considered in the model, making comparison between models difficult.
- A minimum formulation in which the most severely limiting factor alone is assumed to limit growth. This formulation is based on “Liebig’s law of the minimum” which states that the factor in shortest supply will control the growth of algae. The minimum formulation is often used only for nutrient limitation, with a multiplicative formulation for the light limitation factor.

- A harmonic mean formulation that combines the reciprocal of each limiting factor in the following manner:

$$f(Light, Nutrient_1, Nutrient_2, ..., Nutrient_n) = \frac{n}{\frac{1}{f(Light)} + \frac{1}{f(Nutrient_1)} + ... + \frac{1}{f(Nutrient_n)}} \quad \text{Eq. 9-1}$$

  where n = number of limiting factors.

  This formulation is based on an electronic analogy of several resistors in series. The rationale for this formulation is that it includes some interactions between multiple limiting nutrients, but is not as severely limiting as the multiplicative formulation. Under a wide range of conditions, the harmonic mean formulation and minimum formulation produce similar growth response curves (Swartzman and Bentley, 1979 in EPA, 1985).

- An arithmetic mean formulation that uses the average of each limiting factor. The rationale for this formulation is the same as for the harmonic mean formulation. However, this formulation is rarely used since it does not restrict growth enough. For example, the arithmetic mean formulation allows growth even if a critical nutrient such nitrogen is totally absent, as long other nutrients are available.

9.3 Phytoplankton

The growth of phytoplankton is limited to several factors, like described in the following sections.

9.3.1 Nutrient limitation

The model considers nitrogen (ammonia and nitrate) and phosphorus to be the nutrients that limits phytoplankton growth. Nitrate and ammonia are considered in the same pool. But difficulties could be encountered to subtract phytoplankton uptake from the ammonia and nitrate pool and this problem is solved by introduction of the ammonia preference factor (β_{NH4}). The nutrient limitation is expressed in a Michaelis-Menten form, with half saturation constant (K_N). In the case of ammonia and nitrate, the model considers:

$$\Psi(N)_{Phy} = \frac{\mathrm{NH_4} + \mathrm{NO_3}}{K_\mathrm{N} + \mathbf{NH_4} + \mathbf{NO_3}} \qquad \text{Eq. 9-2}$$

where $\Psi(N)_{Phy}$ represents the nutrient limitation due nitrogen presence, NH_4 and NO_3 the ammonia and nitrate concentrations (mg $N.L^{-1}$) and Kn the half-saturation constant for nitrogen limitation (mg $N.L^{-1}$).

In the case of phosphorus the above equation takes the form:

$$\Psi(P)_{Phy} = \frac{\mathrm{PO_4}}{K_\mathrm{P} + \mathrm{PO_4}} \qquad \text{Eq. 9-3}$$

where $\Psi(P)_{Phy}$ represents the nutrient limitation due phosphorus presence, PO_4 the phosphorus concentration (assumed to be completely available as orthophosphate) (mg $P.L^{-1}$) and Kp the half-saturation constant for phosphorus limitation (mg $P.L^{-1}$).

The nutrient limitation factor is given by the minimum of $\Psi(N)_{Phy}$ and $\Psi(P)_{Phy}$.

9.3.2 Temperature limitation

The concept of Thornton and Lessen, (1978) is adopted to represent temperature limitation factor (***Ψ(T)***) on autotrophy and heterotrophy organisms:

$$\Psi(T) = K_A(T) \,.\, K_B(T) \qquad \text{Eq. 9-4}$$

where $K_A(T)$ is defined by:

$$K_A(T) = \frac{K_1 . e^{\gamma_1 . (T - T\min)}}{1 + K_1 . \left(e^{\gamma_1 . (T - T\min)} - 1\right)} \qquad \text{Eq. 9-5}$$

with

$$\gamma_1 = \frac{Ln \dfrac{K_2 (1 - K_1)}{K_1 (1 - K_2)}}{Topt_{\min} - T\min} \qquad \text{Eq. 9-6}$$

where $K_B(T)$ is defined by:

$$K_B(T) = \frac{K_4 . e^{\gamma_2 . (T\max - T)}}{1 + K_4 . \left(e^{\gamma_2 . (T\max - T)} - 1 \right)} \qquad \text{Eq. 9-7}$$

with

$$\gamma_2 = \frac{Ln \dfrac{K_3 (1 - K_4)}{K_4 (1 - K_3)}}{T\max - Topt_{\max}} \qquad \text{Eq. 9-8}$$

$Topt_{min}$ (°C) and $Topt_{max}$ (°C) represent the temperature interval for an optimal process, and Tmax (°C) and Tmin (°C) the maximum and minimum tolerable temperature where processes are completely inhibited. Remaining constants (K_1, K_2, K_3 and K4) control the shape of the response curve of temperature effect; these values are assumed equal for all organisms in this model.

9.3.3 Light limitation

Photosynthesis is possible only when light reaching the algae cell is above certain intensity. This means that phytoplankton is limited to the uppermost layers of the water column where light intensity is sufficient for photosynthesis to occur. The depth to which light will penetrate in water, and hence the depth at which production can occur, is dependent on a number of factors; these include absorption of light by water, the wavelength of light, transparency of water, reflection from the surface of the water, reflection from suspended particles, latitude, and season of the year.

The solar radiation depends on factors such as clouds and dust in the atmosphere and the solar elevation. The calculation of the solar radiation is described in the surface module.

When light strikes the surface of water, a certain amount of light is reflected back; the amount depends on the angle at which the light strikes the surface of water. If the angle from the horizontal is low, a large amount will be reflected. Conversely, the nearer the angle is to 90º (that is

perpendicular to the horizontal surface of the water), the greater will be the penetration and the lesser will be the reflection (Nybakken 1993). The angle at which the light strikes the surface of the water is directly related to the maximum height of the sun above the horizon.

The extinction of light in the marine environment is one of the important water quality variables often addressed by aquatic scientists and oceanographers. The characteristics of the underwater light field itself are a classical subject of oceanographic optics (Rivera, 1997). The available light is one of the primary limiting variables in the growth of submerged flora, besides nutrients and temperature. Light availability is of major importance not only in determining how much plant growth will be but also which kind of species will predominate and which kind will evolve (Rivera, 1997). Vertical light attenuation and its spectral distribution are related to the absorption by the water itself and the following additional components of the water column: photosynthetic organisms, suspended particles and soluble compounds. Modeling light attenuation is the basis to predict the intensity and spectral composition of available light for phototropic populations (Vila *et al,* 1996).

The rate of the light reaction of photosynthesis is strictly dependent on light intensity. Increases in light intensity lead to greater photosynthetic rates until some maximum is reached. At this point the producers cannot use any more light. The enzymes involved in photosynthesis cannot act fast enough to process light quanta any faster, so rate of photosynthesis reaches an asymptote. Increasingly higher light intensities usually inhibit photosynthesis (Valiela, 1995).

9.3.3.1 Light extinction in water

Kirk (1980) defines the inherent optical properties as the absorption, scattering and beam attenuation coefficients of a medium. The absorption coefficient is defined as the fraction absorbed per unit of path length from a parallel beam of monochromatic light directed normal to an infinitesimally thin layer of medium. Similarly, the scattering coefficient is defined as the fraction scattered of the incident parallel beam divided by the path length. The beam attenuation coefficient is defined as the sum of the absorption

and scattering coefficients.

By definition, the incident light field or downward irradiance in a water column refers to the instantaneous value of the down-welling radiant flux in a horizontal unit area.

Kirk (1980) differentiates between downward and upward irradiance, the first being that due to down-welling stream of light and the second duo to the upwelling stream of light. In light extinction studies, the desirable quantity is the down-welling PAR which is referred to as the downward irradiance covering the 400 – 700 nm range of the wave spectrum. The down-welling PAR is attenuated due to both scattering and absorption processes by the optically active components in the water column.

The major light absorbing and scattering components in the water column include dissolved organic substances, dead and living plankton material, suspended inanimate particles, and water itself. These components differ in the way they absorb and scatter downward irradiance across the photosynthetic wave band.

Generally, the strong absorption in inland and estuarine waters is attributed to organic substances, gilvin and/or phytoplankton. On the other hand, scattering, as pointed by Kirk (1980), does not itself “remove” light since a scattered photon is still available for photosynthesis. However, by making the photons follow a zig-zag path, the probability of being absorbed by the absorbing components in the aquatic medium is increased. Hence, with the scattering contribution of suspended particles for example, the vertical attenuation is intensified through this mechanism.

A common method often employed in modeling the extinction of downward irradiance is to consider the influence of the major optically active components separately giving partial extinction coefficients for each component. The sum of all the partial extinction coefficients gives the average extinction coefficient of the water column (Rivera, 1997).

Light extinction in natural waters is affected by four primary groups of substances whose composition and concentration differ in each water body giving different values of the extinction coefficient. Further more, the

extinction coefficient may change with time due to the varying composition and concentrations of the primary factors. These factors, which are referred to as optically active components of the water column, include inanimate suspended solids, dead or living phytoplankton (algae), gilvin and water itself (Rivera, 1997). Parson *et al.* (1984) uses this concept when defining the extinction coefficient in the water column (k) as follows:

$$k=k_w+k_p+k_d+k_s \qquad \text{Eq. 9-9}$$

where k_w, k_p, $k_{d,}$ and k_s represent diffusion and scattering of light energy due to water (w), phytoplankton (p), suspended particles other than phytoplankton (d), and dissolved matter (s), respectively. The suspended particles include many different forms such as clay particles, organic detritus, and organisms varying in size. Each of these extinction coefficients are highly dependent on wavelength, however according to Parson *et al.* (1984), for the purpose of most biological events, the average extinction coefficient in the wavelength of PAR rather than the value at particular wavelengths is probably the most practical.

The partial extinction coefficients can be determined from the specific extinction coefficient and the concentration of the optically active components of the water column by the relation:

$$k_n = \kappa_n c_n \qquad \text{Eq. 9-10}$$

where k_n is the extinction coefficient of a particular component n, κ_n the specific extinction of that component and c_n the observed concentration.

The majority of the water quality models revised (e.g. Vila e Garcia-Gil, 1996 Arhonditsis *et al.* 2000, Napolitano *et al.*, 2000 Nakata *et al.*, 2000, Kawamiya *et al.*, 2000, Humborg *et al.*, 2000, Neuman, 2000, Tett and Wilson, 2000) compute the extinction coefficient considering only phytoplankton self-shading effect. The general form of the established relation is usually like the next equation, with different set of parameters determined according to local measurements.

$$k = k_w + \kappa_{phy} c_{phy} \qquad \text{Eq. 9-11}$$

Cole and Buchak (1995) and Somlyódy and Koncsos (1991) are some examples were the extinction coefficient is computed considering not only the phytoplankton concentration but also sediment concentration.

Each of these specific extinction values can represent a problem of there one in terms of modeling. A usual solution is to develop a relationship based in local measurements that allow us to determine the overall extinction coefficient. This kind of relationship can be dependent on one of the factors already described (usually phytoplankton) but does not specifically distinguish between the chosen factor and other materials. Parson *et al.*, (1984) presents a equation of this kind derived from field observations carried out in the western North Atlantic, which is used by several authors (Yanagi *et al.,* 1997; Miranda 1997). This equation relates the average extinction coefficient (k) to the chlorophyll a concentration (C) for natural phytoplankton community as follows:

$$k = 0.04 + 0.0088C + 0.054C^{2/3} \qquad \text{Eq. 9-12}$$

The coefficients to compute the extinction parameter are determined by the local light conditions of the study area. Portela (1996) following the observations made by Martins e Duffner, (1982) on the Tagus estuary obtained an average value for the extinction coefficient of 4.5 $m^{-}1$ and a median value of 3.4 m^{-1}. Portela (1996) applied a linear regression model to the observed values of extinction coefficient and the concentration of suspended sediments measured in the Tagus estuary in 1980 (Martins e Duffner, 1982). As expected, a close relation between the two variables is observed. The final regression equation is:

$$k=1.24 + 0.036C_{ss} \qquad \text{Eq. 9-13}$$

Another formulation included in the Mohid water quality module, which calculates the effect on light attenuation, depending on phytoplankton and sediment concentration, was presented by Pina (2001):

$$k = 0.04 + 0.0088C + 0.054C^{2/3} + 0.036C_{ss} \qquad \text{Eq. 9-14}$$

9.3.3.2 Phytoplankton reaction to light

The rate of the light reaction of photosynthesis is strictly dependent on light

intensity. Increases in light intensity lead to greater photosynthetic rates until some maximum is reached. At this point the producers cannot use any more light, the enzymes involved in photosynthesis cannot act fast enough to process light quanta any faster, so rate of photosynthesis reaches an asymptote. Increasingly higher light intensities usually inhibit photosynthesis (Valiela, 1995).

During the last decades a considerable amount of research has been carried out on primary productivity modeling (e.g. Steele, 1962; Jassby and Platt, 1976; Platt *et al.*, 1980; Falkowski & Wirick, 1981; Eilers and Peeters, 1988). In most of these works formulations of the relationship between primary productivity and light intensity were proposed and tested against field and/or laboratory data. Most of these equations are empirical, only a few of them being deduced from the physiology of photosynthesis (e.g. Fasham and Platt, 1983; Eilers and Peeters, 1988). These formulations have been used for several years in ecological models.

The light intensity affects only the photosynthesis, its representation use the formulation of Steele (1962) integrated on the depth, Parsons *et al.*., (1995) for this zero-dimensional model and a classic Beer-Lambert function for the light intensity:

$$E(z) = E_0 \cdot e^{(-k(p)z)} \qquad \text{Eq. 9-15}$$

with

$$\Psi(E) = \frac{e^1}{k(p).z} \cdot \left(e^{-\frac{E_0}{Eopt} e^{(-k(p).z)}} - e^{-\frac{E_0}{Eopt}} \right) \qquad \text{Eq. 9-16}$$

E_0 represents the effective solar radiation at the water surface ($W.m^{-2}$), *k(p)* the light extinction factor (m^{-1}), E_{opt} the optimal light intensity for photosynthesis and *z* the depth (m).

9.3.4 Equations

Figure 5-1 represents the internal fluxes of phytoplankton modeled by *Mohid's* water quality module.

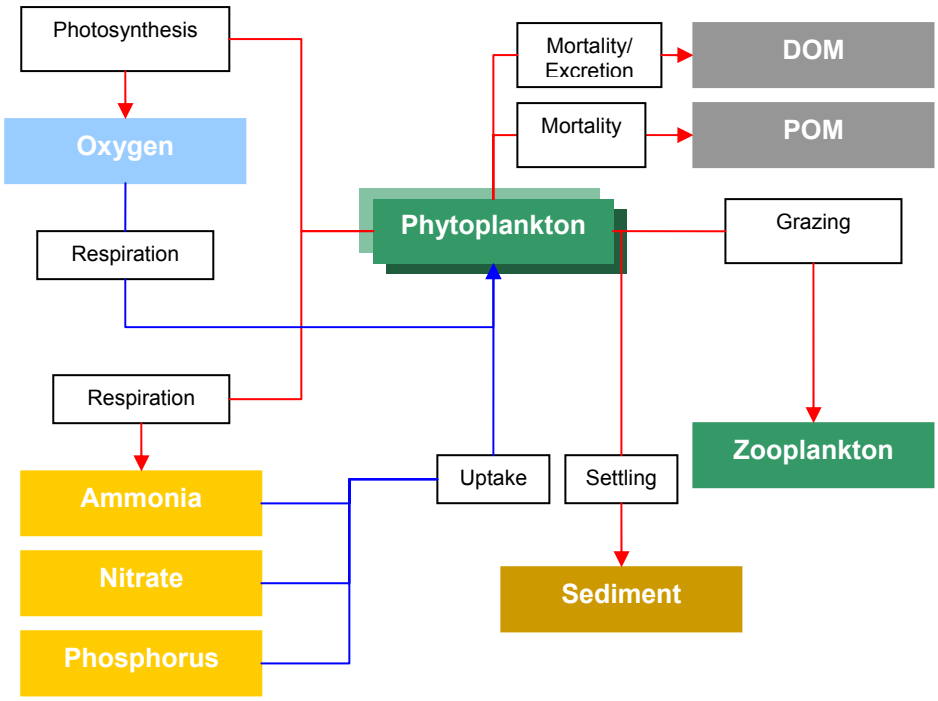

Figure 9-2: Internal Flux of Phytoplankton

Phytoplankton is described in terms of carbon concentration (mgC / l). The model assumes three limitations affecting the maximum phytoplankton growth rate, μmax. Temperature $\Psi(T)$, light effect $\Psi(E)$ and nutrient limitation (minimum of $\Psi(N)_{Phy}$ and $\Psi(P)_{Phy}$), like described in the previous chapter.

The simulation of the phytoplankton is developed with the following considerations: it consumes inorganic nutrients (ammonia and nitrate from the nitrogen cycle and inorganic phosphorus from the phosphorus cycle) depending on their availability. Another factor which influences the growth of phytoplankton is the availability of light as a source of energy for photosynthesis. During the process photosynthesis dissolved oxygen is produced. The respiration process consumes oxygen and produces ammonia. The Excretion of Phytoplankton produces dissolved organic material (Refractory Dissolved Organic Nitrogen, Non-Refractory Dissolved Organic Nitrogen, Refractory Dissolved Organic Phosphorus and Non-Refractory Dissolved Organic Phosphorus). By mortality phytoplankton increases the dissolved organic material and the particulate organic material (Particulate Organic Nitrogen and Particulate Organic

Phosphorus). By the grazing of phytoplankton by zooplankton, the concentration of phytoplankton decreases. The settling process is modeled in the water properties module.

The rate equation of phytoplankton, used by *Mohid*, can be written as:

$$\frac{\partial \Phi_{Phy}}{\partial t} = \left(\mu_{Phy} - r_{Phy} - ex_{Phy} - m_{Phy}\right)\Phi_{Phy} - G \qquad \text{Eq. 9-17}$$

The growth rate, μ_{Phy} (day^{-1}), is given by:

$$\mu_{Phy} = \mu_{\max} \cdot \min(\Psi(N)_{Phy}, \Psi(P)_{Phy}) \cdot \Psi(E)_{Phy} \cdot \Psi(T)_{Phy} \qquad \text{Eq. 9-18}$$

where μ_{max} represents the maximum growth rate.

The respiration, r_{Phy} (day^{-1}), is given by:

$$r_{Phy} = k_{er} \,.\, exp(0.069.T^{o}) + k_p\, \mu_{Phy} \qquad \text{Eq. 9-19}$$

where k_{er} represents the endogenous respiration constant and k_p the photorespiration factor.

The excretion, ex_{Phy} (day^{-1}), is given by:

$$ex_{Phy} = \varepsilon_{Ph}.\, \mu_{Phy}\,(1 - \Psi(E)_{Phy}) \qquad \text{Eq. 9-20}$$

The natural mortality, m_{Phy} (day^{-1}), is given by:

$$m_{Phy} = m_{\max} \cdot \frac{\dfrac{\Phi_{Phy}}{\mu_{Phy}}}{Km + \dfrac{\Phi_{Phy}}{\mu_{Phy}}} \qquad \text{Eq. 9-21}$$

where m_{max} represents the maximum mortality and K_m the mortality half saturation rate.

The grazing, G, is given by:

$$G = \frac{g_z}{E}\Phi_Z \qquad \text{Eq. 9-22}$$

where g_z represents the net growth rate of zooplankton, E the assimilation efficiency and Φ_Z the concentration of zooplankton.

9.4 Zooplankton

Zooplankton is described in terms of carbon concentration (mg C l^{-1}) and the net growth rate, g_z (day^{-1}), is obtained from Ivlev, (1945) adapted by Parsons *et al.*, (1967). Respiration and non-predatory mortality of the zooplankton (day^{-1}), $r_{\tilde{z}}$ and m_{Z_0} are considered functions of temperature, being treated as one variable. The predatory mortality, G_z, depends on the zooplankton concentration.

Figure 9-3 represents the internal flux of zooplankton.

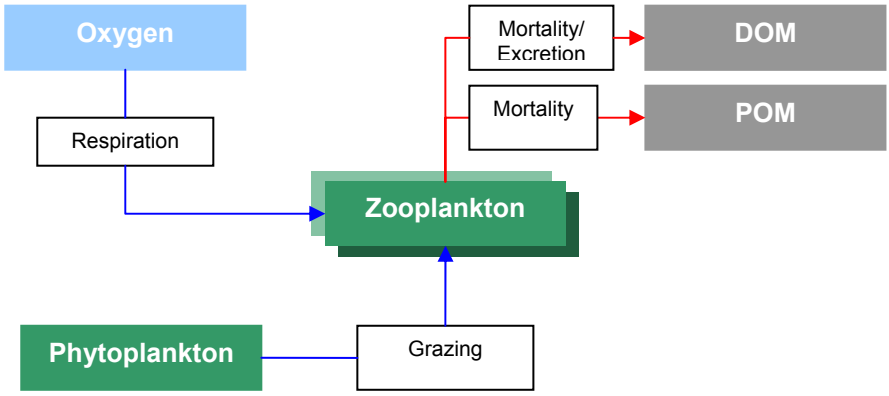

Figure 9-3: Internal Flux of Zooplankton

9.4.1 Equations

The growth of zooplankton is given by:

$$\frac{\partial \Phi_Z}{\partial t} = \left(g_z - r_z - m_z\right) \cdot \Phi_Z \cdot G_Z \qquad \text{Eq. 9-23}$$

The growth rate, g_z (day^{-1}), is given by:

$$g_z = g_{\max} \cdot \left(T_{ref}\right) \cdot \Psi\left(T\right)_Z \cdot \left(1 - e^{-\Lambda\left(\Phi_{Phy} - \Phi_{Phy_0}\right)}\right) \qquad \text{Eq. 9-24}$$

where g_{max} represents the maximum growth rate, Δ stands for the Ivlev

constant, Ω_{Phy0} represents the minimum concentration of phytoplankton for grazing. The temperature limitation is calculated in the same way as for phytoplankton, but with other constants.

The natural mortality and respiration, r_z+m_z (day^{-1}), is given by:

$$r_Z + m_Z = d_Z \cdot \left(T_{ref}\right) \cdot \Psi(T) \qquad \text{Eq. 9-25}$$

where d_z represents the natural mortality and respiration rate.

Grazing, G_z (day^{-1}), is given by:

$$G_z = e_z Z \qquad \text{Eq. 9-26}$$

where e_z represents the predatory mortality rate.

9.5 Nitrogen

In the Mohid water quality module, the nitrogen appears as organic and inorganic nitrogen.

The inorganic nitrogen is divided into ammonia (NH_4), nitrite (NO_2) and nitrate (NO_3).

The organic nitrogen is divided into particulate organic nitrogen (PON), dissolved organic nitrogen non refractory (DONnr) and dissolved organic nitrogen refractory (DONre). DONnr includes small molecular substrates, assumed to be degraded in the day of production and DONre with a longer turn over.

9.5.1 Ammonia

The sources of ammonia are the organic forms of nitrogen (PON, DONnr and DONre) due to decay and phytoplankton due to the dark respiration process. The sinks of ammonia are nitrite (nitrification) and phytoplankton (uptake).

Figure 9-4 represents the internal fluxes of ammonia modeled by *Mohid's* water quality module.

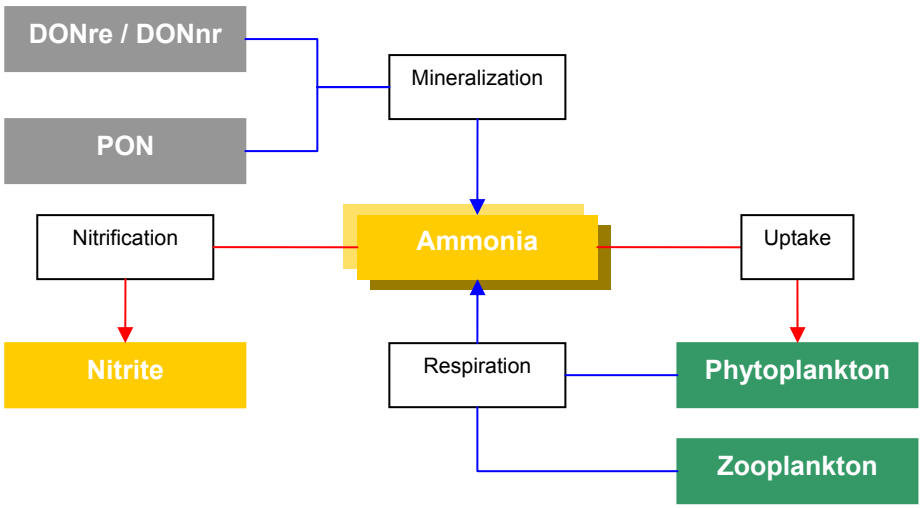

Figure 9-4: Internal Flux of Ammonia

The rate equation of ammonia is given by:

$$\frac{\partial \Phi_{NH4}}{\partial t} = \left(f_{in/Phy} ex_{Phy} - \mu_{NH4}\right)\Phi_{Phy} + f_{in/Z} ex_z \Phi_z + \varphi_{Nre}\Phi_{DONre} + \varphi_{Nnr}\Phi_{DONnr} + f_{orgP/Phy}\varphi_{det}\Phi_{PON} \quad \text{Eq. 9-27}$$

The assimilation rate of NH_4, μ_{NH4}, is given by:

$$\mu_{NH4} = \beta_{NH4}\alpha_{N:C}\mu_{Phy} \quad \text{Eq. 9-28}$$

where β_{NH4} is the ammonia preference factor given by:

$$\beta_{NH4} = \frac{\Phi_{NH_4}\cdot\Phi_{NO_3}}{\left(K_N + \Phi_{NH_4}\right)\left(K_N + \Phi_{NO_3}\right)} \cdot \frac{\Phi_{NH_4}\cdot K_N}{\left(K_N + \Phi_{NH_4}\right)\left(K_N + \Phi_{NO_3}\right)} \quad \text{Eq. 9-29}$$

and $\alpha_{N:C}$ represents the Redfield ratio between N:C.

The mineralization rate of DONre, φ_{Nre} is given by:

$$\varphi_{Nre} = M_{DONre}\theta_{DONre}(T - T_{ref})\frac{\Phi_{Phy}}{K_{PhyNut\,\mathrm{Re}\,ge} + \Phi_{Phy}} \quad \text{Eq. 9-30}$$

where

M_{DONre} – reference rate for the mineralization of DONre

θ_{DONre} – temperature coefficient for the mineralization of DONre

T_{ref} – reference temperature

$K_{PhyNutRege}$ – half saturation constant for the regeneration of phytoplankton

The mineralization rate of DONnr, φ_{Nnr} is given by:

$$\varphi_{Nnr} = M_{DONnr}\theta_{DONnr}(T - T_{ref}) \qquad \text{Eq. 9-31}$$

where

M_{DONnr} – reference rate for the mineralization of DONnr

θ_{DONnr} – temperature coefficient for the mineralization of DONnr

The dissolution rate of PON, φ_{det}, is given by:

$$\varphi_{\det} = M_{\det}\theta_{\det}(T - T_{ref}) \qquad \text{Eq. 9-32}$$

where

M_{det} – reference rate for the dissolution of PON

θ_{det} – temperature coefficient for the dissolution

9.5.2 Nitrite

The source of nitrite, modeled by *Mohid*, is ammonia and the sink is nitrate. Figure 9-5 represents the internal fluxes of nitrite modeled by *Mohid's* water quality module.

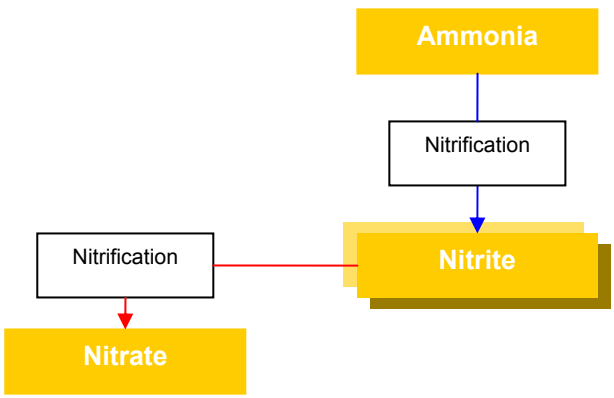

Figure 9-5: Internal Flux of Nitrite

The rate equation of nitrite is given by:

$$\frac{\partial \Phi_{NO2}}{\partial t} = \varphi_{2N}\Phi_{NH4} - \varphi_{2N}\phi_{NO2} \qquad \text{Eq. 9-33}$$

with the rate of nitrification, φ_{2N} is given by:

$$\varphi_{2N} = M_{nit}\theta_{nit}\left(T - T_{ref}\right)\frac{\Phi_{O2}}{K_{nit} + \Phi_{O2}} \qquad \text{Eq. 9-34}$$

where

M_{nit} – reference rate of nitrification

θ_{nit} – temperature coefficient for nitrification

K_{nit} – half saturation constant for nitrification

9.5.3 Nitrate

The source of nitrate, modeled by *Mohid*, is nitrite and the sink the uptake by phytoplankton. Figure 9-6 represents the internal fluxes of nitrate modeled by *Mohid's* water quality module.

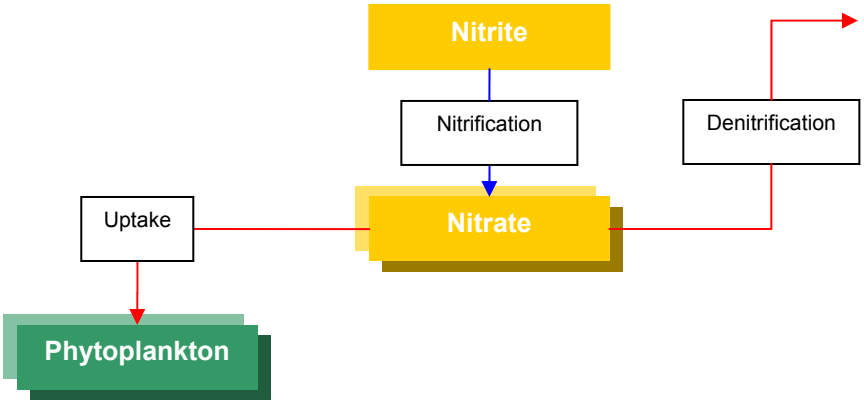

Figure 9-6: Internal Flux of Nitrate

The rate equation of nitrate is given by:

$$\frac{\partial \Phi_{NO3}}{\partial t} = \varphi_{2N}\Phi_{No2} - \varphi_{2N}\phi_{NO3} - \mu_{NO3} \qquad \text{Eq. 9-35}$$

The assimilation rate of $N0_3$, μ_{NO3}, is given by:

$$\mu_{NO3} = (1 - \beta_{NH4})\alpha_{N:C}\mu_{Phy} \qquad \text{Eq. 9-36}$$

9.5.4 Particulate organic nitrogen – PON

The sources of PON are the mortality of phytoplankton and zooplankton and the sinks are the mineralization to ammonia and the decomposition to DONre.

Figure 9-7 represents the internal fluxes of PON modeled by *Mohid's* water quality module.

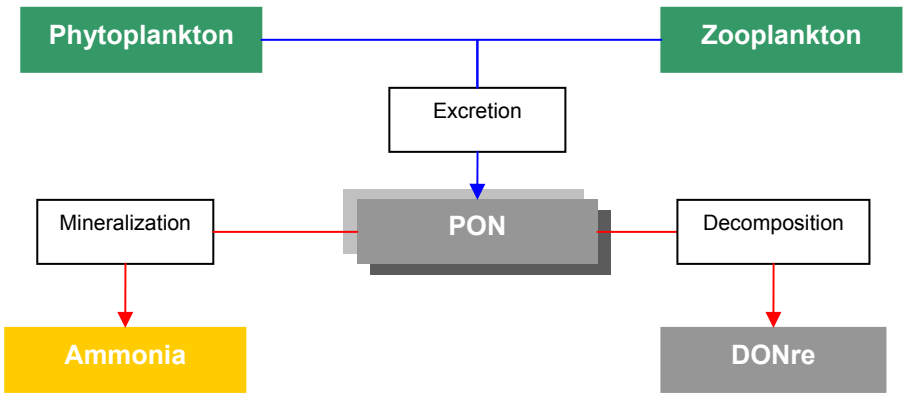

Figure 9-7: Internal Flux of PON

The rate equation of the PON is given by:

$$\frac{\partial \Phi_{PON}}{\partial t} = \left[\left(1 - f_{orgD/Phy}\right)\left(1 - f_{in/Phy}\right)ex_{Phy} + m_{Phy}\right]\Phi_{Phy} +$$

$$\left[\left(1 - f_{orgD/Z}\right)\left(1 - f_{in/Z}\right)ex_{Z} + m_{Z}\right]\Phi_{Z} - \varphi_{\det}\Phi_{PON} \qquad \text{Eq. 9-37}$$

All variables have the same meaning as in the previous paragraphs.

9.5.5 Dissolved organic nitrogen non refractory – DONnr

The sources of DONnr are the mortality and the excretions of phytoplankton and zooplankton and the sinks are the mineralization to ammonia.

Figure 9-8 represents the internal fluxes of DONnr modeled by *Mohid's* water quality module.

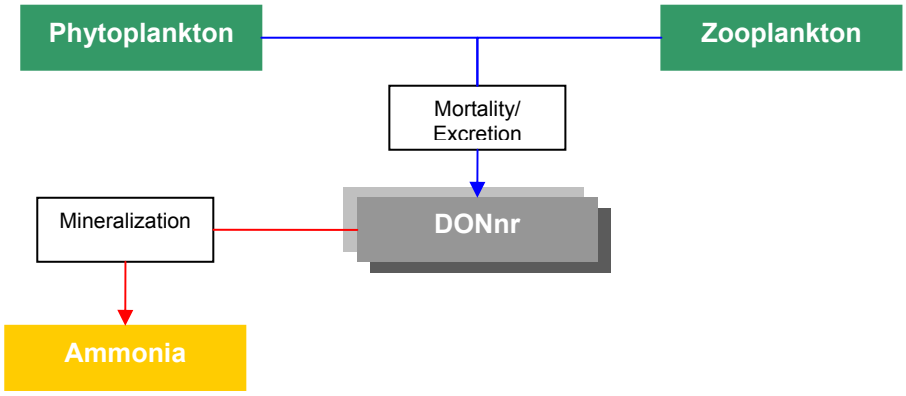

Figure 9-8: Internal Flux of DONnr

The rate equation of the DONnr is given by:

$$\frac{\partial \Phi_{DONnr}}{\partial t} = f_{orgD/Phy}(1 - f_{in/Phy}) ex_{Phy} \Phi_{Phy}$$

$$+ f_{orgD/Z}(1 - f_{in/Z}) ex_{Z} \Phi_{Z} - \varphi_{Nnr} \Phi_{DONnr} \qquad \text{Eq. 9-38}$$

All variables have the same meaning as in the previous paragraphs.

9.5.6 Dissolved organic nitrogen refractory – DONre

The source of DONre is the decomposition of the PON and the sink is the mineralization to ammonia.

Figure 9-9 represents the internal fluxes of DONre modeled by *Mohid's* water quality module.

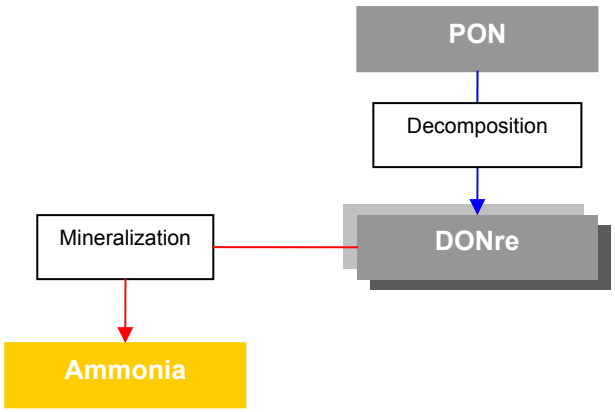

Figure 9-9: Internal Flux of DONre

The rate equation of the DONre is given by:

$$\frac{\partial \Phi_{DONre}}{\partial t} = \varphi_{\det} \Phi_{PON} (1 - f_{orgP/Phy}) - \varphi_{Nr} \Phi_{DONre} \qquad \text{Eq. 9-39}$$

All variables have the same meaning as in the previous paragraphs.

9.6 Phosphorus

In the Mohid water quality module, phosphorus appears, like nitrogen, in an organic and an inorganic form.

The inorganic phosphorus is assumed to be available as orthophosphate (PO_4) for uptake by phytoplankton.

The organic phosphorus is divided into particulate organic phosphorus (POP), dissolved organic phosphorus non refractory (DOPnr) and dissolved organic phosphorus refractory (DOPre). The rate equations of phosphorus are implemented in the same way as the nitrogen cycle, except that there is just one compartment of inorganic phosphorus.

9.6.1 Inorganic Phosphorus

Figure 9-10 represents the internal fluxes of inorganic phosphorus modeled by *Mohid's* water quality module.

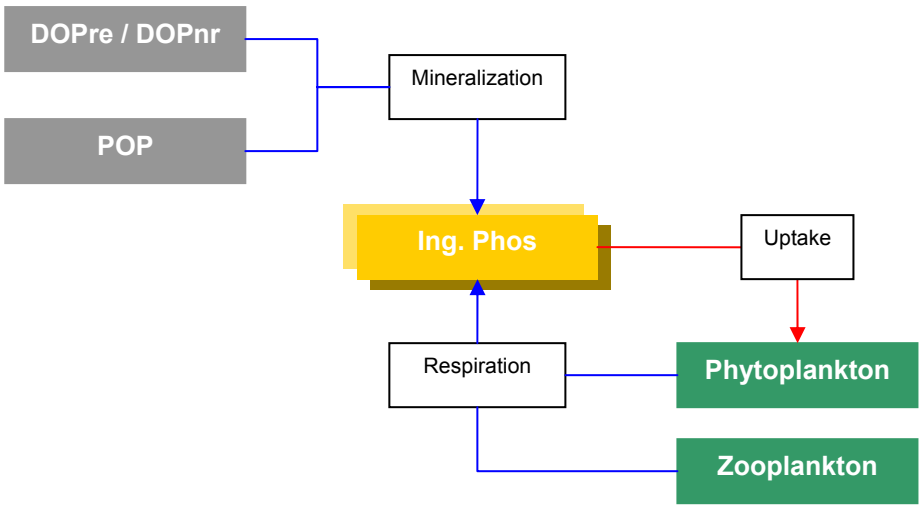

Figure 9-10: Internal Flux of Inorganic Phosphorus

The rate equation of inorganic phosphorus is given by:

$$\frac{\partial \Phi_{PO4}}{\partial t} = (f_{in/Phy} ex_{Phy} - \mu_{PO4})\Phi_{Phy} + f_{in/Z} ex_z \Phi_z + \varphi_{Pre} \Phi_{DOPre} + \varphi_{Pnr} \Phi_{DOPnr} + f_{orgP/Phy} \varphi_{det} \Phi_{POP} \quad \text{Eq. 9-40}$$

The assimilation rate of PO_4, μ_{PO4}, is given by:

$$\mu_{PO4} = \alpha_{N:C} \mu_{Phy} \quad \text{Eq. 9-41}$$

α_{Phy} represents the Redfield ratio between N:P.

9.6.2 Particulate organic phosphorus - POP

9.6.3 Dissolved organic phosphorus non refractory - DOPnr

9.6.4 Dissolved organic phosphorus refractory - DOPre

9.7 Oxygen

Figure 9-11 represents the internal fluxes of oxygen by *Mohid's* water quality module.

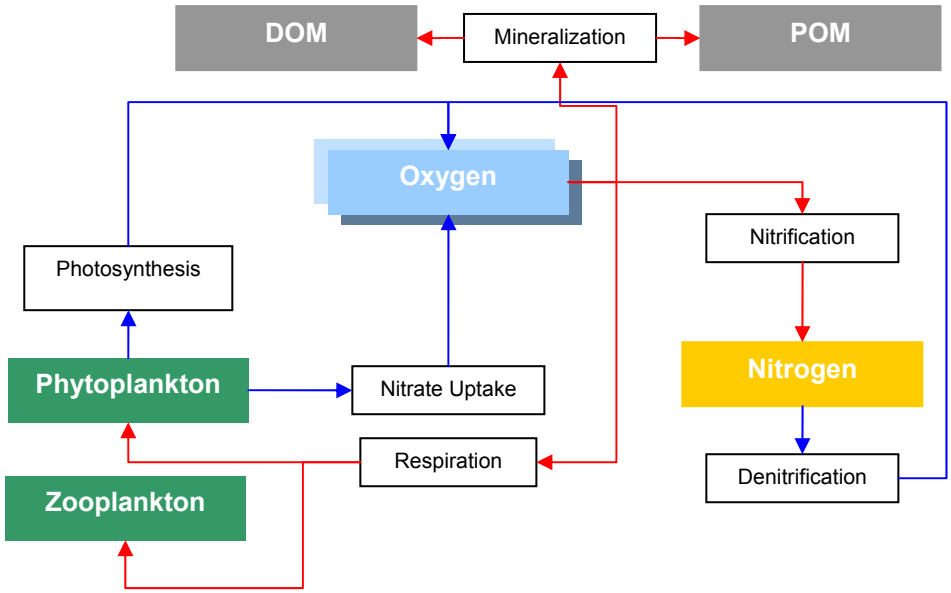

Figure 9-11: Internal Flux of Inorganic Oxygen

$$\frac{\partial \Phi_O}{\partial t} = \left(\mu_{phy}\alpha_{O:C} + \mu_{phy}\alpha_{O:N}\alpha_{N:C}\left(1-\beta_{NH4}\right) - \alpha_{O:C}r_{Phy}\right)\Phi_{Phy} + r_z\alpha_{O:C}\Phi_{Zoo} + \varphi_{2N}\alpha_{N:O}\Phi_{NH4} - \left(\begin{matrix}\alpha_{MinO:N}\varphi_{Nre}\Phi_{DONre} + \alpha_{MinO:N}\varphi_{Nnr}\Phi_{DONnr} + \alpha_{MinO:N}\varphi_{\det}\Phi_{PON} + \alpha_{MinO:P}\varphi_{\Pr e}\Phi_{DO\Pr e} + \\ \alpha_{MinO:P}\varphi_{Pnr}\Phi_{DOPnr} + \alpha_{MinO:P}\varphi_{\det}\Phi_{POP}\end{matrix}\right)\Phi_O \quad \text{Eq. 9-42}$$

$\alpha_{MinO:N}$ Mineralization oxygen/ nitrogen ratio

$\alpha_{MinO:P}$ Mineralization oxygen/ phosphorus ratio

10 The Surface Module

10.1 Introduction

The surface module stores the boundary conditions at the surface of the water column. These boundary conditions can be divided in two types of boundary condition. One type of boundary condition which are given directly be the user, usually meteorological data (wind velocity, air temperature, dew point, evaporation, cloud cover) or boundary conditions calculated automatically by the model from the meteorological data/conditions of the water column (wind stress, solar radiation, latent heat, infrared radiation, sensible heat, oxygen flux). The information flux between the surface module and other modules is shown in Figure 10-1.

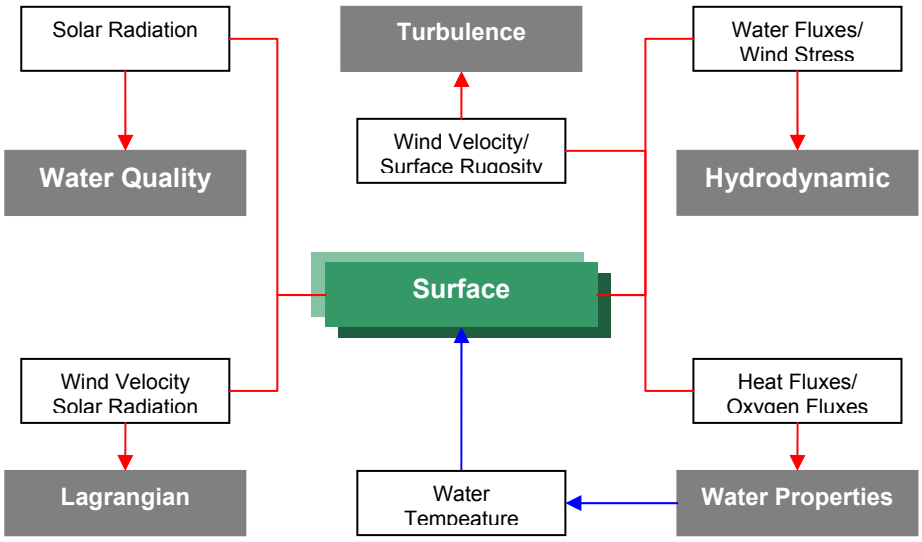

Figure 10-1: Information flux between the Surface Module and other modules

10.2 Wind

Wind stress is calculated according to a quadratic friction law:

$$\vec{\tau w} = C_D \rho_a \vec{W} \left| \vec{W} \right| \qquad \text{Eq. 10-1}$$

where C_D is a drag coefficient that is function of the wind speed, ρ_a is air

density and *W* is the wind speed at a height of 10 m over the sea surface.

The drag coefficient is computed according to Large and Pond [1981]:

$$C_D = 1.14e^{-3} \text{ (W<10m/s)} \quad \text{Eq. 10-2}$$

$$C_D = 4.4e^{-4} + 6.5e^{-5}\,\vec{W}\left|\vec{W}\right| \text{ (10m/s<W<26m/s)} \quad \text{Eq. 10-3}$$

10.3 Heat fluxes

The heat fluxes at the surface can be separated into five distinctive fluxes: solar shortwave radiation, atmospheric long-wave radiation, water long-wave radiation, sensible heat flux and latent heat flux. These fluxes can be grouped into two ways: in (*i*) radiative fluxes (first three fluxes) and (*ii*) non-radiative fluxes (last two fluxes) or in (*iii*) fluxes independent of the water temperature (first two fluxes) and in (*iv*) fluxes dependent of the water temperature (last three fluxes).

10.3.1 Solar radiation

Solar radiation is an important ecological parameter, and is often the key driving force in ecological processes (Brock, 1981). The solar radiation flux of short wavelength is compute by:

$$Q = Q_0 A_t (1-0.65 C_n^2)(1-R_s) \quad \text{Eq. 10-4}$$

where Q_0 is the solar radiation flux on top atmosphere (Wm^2), A_t the coefficient for atmospheric transmission, C_n the cloud cover percentage and R_s stands for albedo (0.055). The solar radiation flux on top atmosphere can be expressed as:

$$Q_0 = \frac{I_0}{r^2} senz \quad \text{Eq. 10-5}$$

where I_0 stands for the solar constant which is the energy received per unit time, at Earth's mean distance from the Sun, outside the atmosphere, a standard value, used is 1353 Wm^{-2} (Brock, 1981), *r* stands for the radious vector and z stands for the solar high.

10.3.1.1 Radius vector, *r*

During its revolution around the Sun, the Earth's distance varies with time of year by 3.0%, duo to the Earth's eccentric orbit. This eccentricity influences in a minor way the amount of solar radiation impinging on the Earth's surface. The radius vector of Earth, *r*, expresses this ellipticity and can be calculated approximately from the following equation (Nicholls and Child, 1979 in Brock, 1981):

$$r = 1.0 + 0.017\cos\left[2\pi\frac{(186 - d)}{365}\right] \qquad \text{Eq. 10-6}$$

where *d* stands for Julian Day.

10.3.1.2 Solar High

Solar radiation at any location on Earth is influenced by the motions which the Earth makes in relation to the Sun. The Earth is tilted 23.45º from the plane of the Earth's orbit. The declination of Earth is the angular distance at solar noon between the Sun and the Equator, north-positive. Declination depends only on the day of the year, and will be opposite in the Southern Hemisphere. The declination is obtained precisely from ephemeris tables, but can be calculated close enough for all practical purposes from the equation given by Cooper (1969 in Brock, 1981):

$$D1(\text{declination}) = 23.45 \sin[2\pi(284 + d)/365] \qquad \text{Eq. 10-7}$$

The other major motion is the daily rotation of the Earth around itself. The Earth moves 15º per hour and the sunset (or sunrise) hour –angle, W1, is the angle between the setting Sun and the south point. The value W1 can be calculated if the latitude (L) and declination are known:

$$W1 = \arccos(-\tan(L)\tan(D1)) \qquad \text{Eq. 10-8}$$

In this equation, if L and D1 are in degrees then W1 will be given in degrees. From W1, the daylength in hours, L1, can be calculated from the equations:

$$\text{Sunrise} = 12 - \tfrac{1}{2} L1 \qquad \text{Eq. 10-9}$$

$$Sunset = 12 + ½ L1 \quad \text{Eq. 10-10}$$

The hour-angle at any given time can be calculated from one of the following equations:

$$W2 = (T+12)*\pi/12,\ T<12 \quad \text{Eq. 10-11}$$

$$W2 = (T-12)*\pi/12,\ T>12$$

Where T is the time (h) from midnight.

The Zenith angle or angular elevation of the Sun above the horizon, Z, can be calculated if the declination, D1, the latitude, L1, and the hour-angle, W2, are known:

$$Cos\ (Z) = sin(D1)sin(L) + cos(D1)cos(L)cos(W2) \quad \text{Eq. 10-12}$$

As a consequence of attenuation, radiation has two distinct directional properties when it reaches the ground.

10.3.1.3 Direct Radiation

Direct radiation arrives from the direction of the solar disc and includes a small component scattered directly forward. The term diffuse describes all other scattered radiation received from the blue sky and from clouds, either by reflection or by transmission. Direct radiation at the ground, measured at right angles to the beam, rarely exceeds 75% of the Solar Constant, i.e. about 1030Wm^{-2}. The minimum loss of 25% is attributable to molecular scattering and to absorption in almost equal proportions. (Monteith and Unsworth, 1990)

10.3.1.4 Diffuse radiation

Beneath a clean, cloudless atmosphere, the absolute amount of diffuse radiation increases to a maximum somewhat less then 200 Wm^2 when the zenith angle of the sun (Z) is less then 50º and the ratio of diffuse (Q_{dif}) to total radiation (Q_0) falls between 0.1 and 0.15. With increasing cloud amount also, Q_{dif}/ Q_0 increases and reaches unity when the sun is obscured by dense cloud: but the absolute level of Q_d is maximal when

cloud cover is about 50%.

The coefficient for atmospheric transmission is computed by the method followed by Rosati and Miyakoda (1988 in Portela, 1996):

$$A_t = A_{dir} + A_{dif} \qquad \text{Eq. 10-13}$$

where A_{dir} is the direct fraction and A_{dif} is the diffuse fraction of solar radition on top atmosphere that reaches the surface under a clear sky.

The direct fraction A_{dir} is given by:

$$A_{dir} = \tau^m \qquad \text{Eq. 10-14}$$

where τ = 0.74 is atmospheric transmission coefficient for direct radiation and *m* the sectional mass, compute by the following expression:

$$m = 1/\ \text{sen}\ (Z) \qquad \text{Eq. 10-15}$$

where is the zenith angle in radians.

The diffuse fraction A_{dif} is given by:

$$A_{dif} = \frac{1 - A_a - A_{dir}}{2} \qquad \text{Eq. 10-16}$$

were A_0= 0.09 is the absorption coefficient due to water vapour and ozone.

10.3.2 Infrared radiation flux

The infrared radiation flux is computed in concordance with the *Stefan-Boltzman* law:

$$R_{br} = \varepsilon * \sigma * (273.15 + T_w)^4 \qquad \text{Eq. 10-17}$$

where R_{br} represents the infrared radiation (W/m^2), ε the emissivity of water (0.97), σ the Stefan-Boltzman constant ($5.669*10^{-08}$ $W/m^2/K^4$) and T_w the water temperature.

10.3.3 Latent heat flux

The latent heat flux decreases the heat inside the water body. It represents the quantity of heat for the evaporation. The equation implemented in the model *Mohid* is known by the law of *Dalton:*

$$H_L = (19.0 + 0.95U_w^2) * (e_{s,w} - r_h * e_{s,a}) \qquad \text{Eq. 10-18}$$

where H_L represents the latent heat flux (m/s), $e_{s,w}$ water pressure of saturation (mmHg), r_h for the relative humidity and $e_{s,a}$ the air pressure of saturation.

The model just considers the latent heat in the case of evaporation. In the inverse process, the model considers that the heat gain remains in the atmosphere.

10.3.4 Sensible heat flux

The difference between the air temperature and the water temperature is responsible for the sensible heat flux. The equation implemented in the model *Mohid* is known by the law of *Bowen:*

$$H_S = C_b * (19.0 + 0.95 * U_w^2) * (T_w - T_a) \qquad \text{Eq. 10-19}$$

Where H_s represents the sensible heat flux (W/m^2), C_b is the *Bowen's* coeficient (0.47mmHg/K), U_w the wind speed 10m above the surface of the water, T_w the water temerature and T_a the air temperature (K).

10.4 Gas flux

Actually just the oxygen flux is implemented. The formula used is indicated below:

$$K_L = \alpha U_W{}^{\beta} \qquad \text{Eq. 10-20}$$

where K_L represents the velocity of the gas transfer (m/s), α and β are coefficients depending in on the wind velocity, U_w:

α = 0.2 if W <3.5 and α = 0.057 if W > 3.5

β = 1.0 if W <3.5 and β = 2.0 if W >3.5

11 The Bottom Module

11.1 Introduction

The bottom module computes boundary conditions at the bottom of the water column. It computes shear stress as a boundary condition to the hydrodynamic and turbulence modules. It is also responsible for computing fluxes at the water-sediment interface, managing boundary conditions to both the water column properties and the sediment column properties.

Both in the water column or in the sediment column, properties can be either dissolved or particulate. The evolution of dissolved properties depends greatly on the water fluxes, both in the water column and in the sediment interstitial water. Particulate properties evolution in the water column depends also on the water fluxes and on settling velocity. Once deposited in the bottom they can either stay there or be resuspended back to the water column. If they stay there for a determined period of time, they can become part of the sediment compartment by consolidation.

11.2 Erosion and deposition

For particulate properties at the bottom, a flux term, F_b, (mass of sediment per unit bed area per unit time) is defined, corresponding to a source or sink for the suspended particulate matter in conditions of erosion or deposition, respectively. Consequently, at the bottom:

$$F_b = E - D$$

where E and D are respectively the erosion and deposition fluxes. It is assumed that, when bottom shear stress is smaller than a critical value for deposition, there is addition of matter to the bottom, and, when the bottom shear is higher than a critical value, erosion occurs. Between those values, erosion and deposition balance each other.

11.2.1 Erosion flux

The erosion algorithm used is based on the classical approach of Partheniades, (1965). Erosion occurs when the bottom shear stress

exceeds the threshold of erosion. The flux of eroded matter is given by:

$$\frac{dM_E}{dt} = E\left(\frac{\tau}{\tau_E} - 1\right) \quad \text{for} \quad \tau > \tau_E \,, \qquad \text{Eq. 11-1}$$

$$\frac{dM_E}{dt} = 0 \quad \text{for} \quad \tau < \tau_E \,, \qquad \text{Eq. 11-2}$$

where τ is the bed shear stress, τ_E is a critical shear stress for erosion and E is the erosion constant ($kgm^{-2}s^{-1}$).

As this algorithm was developed specifically for cohesive sediment modelling, when computing other particulate properties fluxes at the bed, the erosion constant cannot be the same. Thus it is computed a specific proportionality factor for the erosion constant, E_{prop}, for each property, relating the quantity of property to the quantity of cohesive sediment deposited in the bed.

$$E_{prop} = E\left(\frac{M_{property}}{M_{sediment}}\right) \qquad \text{Eq. 11-3}$$

This way, critical shear stress values are considered equal for all particulate properties, being the specific erosion constant the differentiating factor.

11.2.2 Deposition flux

Regarding the deposition flux, this can be defined as:

$$F_p = \frac{dm}{dt} = -pW_S C \qquad \text{Eq. 11-4}$$

where p is the probability of sediment deposition, W_S the settling velocity and C the near-bed cohesive sediment concentration. The probability of deposition (Krone, 1962), is defined as:

$$p = (1 - \frac{\tau_b}{\tau_{cd}})$$ Eq. 11-5

where τ_b and τ_{cd} are the bottom shear stress and a critical shear stress for deposition respectively. This concept reflects the fact that the deposition of flocks is controlled by near-bed. For a flock to stick to the bed it must be strong enough to withstand the near bed shear stress.

The deposition algorithm (Krone, 1962), like the erosion algorithm, is based on the assumption that deposition and erosion never occur simultaneously, i.e. a particle reaching the bottom has a probability of remaining there that varies between 0 and 1 as the bottom shear stress varies between its upper limit for deposition and zero respectively. Deposition is calculated as the product of the settling flux and the probability of a particle to remain on the bed:

$$\frac{dM_D}{dt} = (CW_S)_B (1 - \frac{\tau}{\tau_D}) \quad \text{for} \quad \tau < \tau_D$$ Eq. 11-6

$$\frac{dM_D}{dt} = 0 \quad \text{for} \quad \tau > \tau_D$$ Eq. 11-7

where τ_D is the critical stress for deposition. The critical shear stress for deposition, τ_D, depends mainly on the size of the flocks.

11.3 Waves tension

Waves exert friction forces at the bed during propagation. The bed shear stress, which is important for wave damping and sediment entrainment, is related to the friction coefficient by:

$$\tau_w = \frac{1}{2} \rho f_w U_\delta^2$$ Eq. 11-8

In which:

τ_w Instantaneous bed-shear stress [N/m^2]

f_w Friction coefficient [dimensionless]

U_δ Instantaneous fluid velocity just outside boundary layer [m/s]

ρ Fluid density [kg/m^3]

The friction factor f_w is assumed to be constant over the wave cycle and is determined from the peak values as:

$$f_w = 2\tau_w / \left(\rho U_\delta^2\right) \qquad \text{Eq. 11-9}$$

The time-average (over a wave cycle) bed shear stress is:

$$\hat{\tau}_w = \frac{1}{4}\rho f_w \hat{U}_\delta^2 \qquad \text{Eq. 11-10}$$

In the rough turbulent regime Jonsson (1966 in van Rijn, 1989) proposed:

$$f_w = \exp\left[-6 + 5.2\left(\frac{\hat{A}_\delta}{k_s}\right)^{-0.19}\right] \qquad \text{Eq. 11-11}$$

$f_{w,max}$=0.3for$\left(\frac{\hat{A}_\delta}{k_s}\right) \le 1.57$

where k_s stands for bed roughness [m]

11.3.1 Wave parameters

Applying linear wave theory, the peak value of the orbital excursion ($\hat{A}_\delta$)

and velocity ($\hat{U}_\delta$) at the edge of the wave boundary layer can be expressed as:

$$\hat{A}_\delta = \frac{H}{\sinh(kh)} \qquad \text{Eq. 11-12}$$

$$\hat{U}_\delta = \hat{A}_\delta \varpi = \frac{H\Pi}{T\sinh(kh)} \qquad \text{Eq. 11-13}$$

in which:

$\varpi = 2\Pi / T$	Angular velocity [rad/s]
$k = 2\Pi / L$	Wave number [rad/m]
H	Wave height [m]
$L = \left(gt^2 / 2\Pi\right)\tanh(kh)$	Wave length [m]
T	Wave period [s]
H	Water depth [m]

Linear wave theory is generally applied to determine the near-bed velocities. In case of symmetrical (sinusoidal) small-amplitude waves in relatively deep water this theory yields correct results. When waves are approaching shallower waters, the waves will be distorted leading to asymmetrical wave profiles and higher order wave theories are basically necessary to determine the near-bed velocities. Surprisingly, comparisons of measured velocities and computed velocities according to linear wave theory show reasonably good results in shallow water.

11.3.2 Bed roughness

Wave ripples are formed once the oscillatory motion is of sufficient strength to cause general movement of the surface particles. The height and length of the ripples grow until a stable ripple is obtained depending on the prevailing conditions. When fully developed riples are generally two-

dimensional, regular and have a sinusoidal shape. At larger velocities the flow separeted from the riples and strong eddies are generated which can sweep the particles from the troughs to crests and vice-versa.

van Rijn (1989) relates the ripple height (Δ_r)and length (λ_r) to the peak value of the orbital excursion ($\hat{A}_\delta$) and a particle mobility parameter (ψ), as follows:

$$\frac{\Delta_r}{\hat{A}_\delta}, \frac{\Delta_r}{\lambda_r} = F(\Psi) \qquad \text{Eq. 11-14}$$

in which:

$$\Psi = \left(\hat{U}_\delta\right)^2 / [(\rho_{rel})gd_{50}] \qquad \text{Eq. 11-15}$$

and, ρ_{rel} relative density $\left(\frac{\rho_{sand} - \rho_{water}}{\rho_{water}}\right)$.

Symbol	Name	Value	Unit
ρ_{sand}	Sand density	2.3	
ρ_{water}	Water density	1.025	
g	Gravity	9.8	ms^{-2}
d_{50}	Particle diameter	0.002	m
d_{90}	Particle diameter	0.003	m

van Rijn (1989) proposes the following relationships for irregular waves:

$$\frac{\Delta_r}{\hat{A}_\delta} = 0.22 \qquad \text{for } \Psi \le 10$$

$$\frac{\Delta_r}{\hat{A}_\delta} = 2.8\times10^{-13}\left(250-\Psi\right)^5 \qquad \text{for } 10 \le \Psi \le 250$$

$$\frac{\Delta_r}{\hat{A}_\delta} = 0 \qquad \text{for } \Psi \ge 250$$

Eq. 11-16

$$\frac{\Delta_r}{\lambda_r} = 0.18 \qquad \text{for } \Psi \le 10$$

$$\frac{\Delta_r}{\lambda_r} = 2\times10^{-7}\left(250-\Psi\right)^{2.5} \qquad \text{for } 10 \le \Psi \le 250$$

$$\frac{\Delta_r}{\lambda_r} = 0 \qquad \text{for } \Psi \ge 250$$

The proposed expressions for ripple steepness $\frac{\Delta_r}{\lambda_r}$ are valid for non-breaking wave conditions. In case of breaking wave conditions the mobility parameter (ψ) will, in general, be larger than 250 yielding sheet flow over a flat bed. In spilling breaking waves this may be realistic. However, in plunging breaking waves the interaction of the waves with bed is so vigorously that rather irregular bed surface may be generated.

Nikuradse (1932, in van Rijn ,1989) introduced the concept of an equivalent or effective sand roughness height to simulate the roughness of arbitrary roughness elements of the boundary. In case of a movable bed consisting of sediments the effective roughness mainly consists of grain roughness generated by skin friction forces and of form roughness generated by pressure forces acting on the bed forms.

Grain roughness is dominant when the bed is plane or when the peak orbital excursion at the bed is smaller than the ripple length.

Ripples are here in defined as bed forms with length smaller than the water

depth. Riples are the dominant bed forms generated by oscillatory flow. When the near-bed orbital excursion is larger than the riple length, the ripples are the dominant roughness (form roughness) elements on the bed. Assuming hydraulic rough flow and a dominant form roughness, van Rijn (1989) proposes the following values:

For grain roughness

$$k_{s,w}^{grain} = 3d_{90} \quad \text{for } \Psi < 250 \qquad \text{Eq. 11-17}$$

$$k_{s,w}^{grain} = 3(0.04\Psi - 9)d_{90} \quad \text{for } \Psi \geq 250$$

For form roughness

$$k_{s,w}^{form} = 16\Delta_r \frac{\Delta_r}{\lambda_r} \quad \text{for } \Psi < 250 \qquad \text{Eq. 11-18}$$

$$k_{s,w}^{form} = 0 \quad \text{for } \Psi \geq 250$$

Finally bed roughness is determined

$$k_s = \min\left[\left(k_{s,w}^{form} + k_{s,w}^{grain}\right), 0.010\right] \quad [m] \qquad \text{Eq. 11-19}$$

11.4 Consolidation

The consolidation flux can only be computed if the sediment modules are active. The flux is computed by specifying a consolidation rate that is applied over the cohesive sediment mass available. To compute this consolidation flux in each cell, first it is computed the average mass availability during the consolidation integration step. If this average value is higher than the value of mass available in the beginning of the integration step, then it is considered that in this cell, during the integration step, the deposition flux outbalanced the erosion flux, meaning that the sediment

flocks stood there long enough to become consolidated. The algorithm follows:

$$M_{average} = \frac{\sum_{t=t_o}^{t_{consolidation}} M_t \times dt}{dt_{consolidation}} \quad \text{Eq. 11-20}$$

$$\frac{dM}{dt} = Mr_c, \text{ for } M_{average} > M_{t_o} \quad \text{Eq. 11-21}$$

where $M_{average}$ is the average mass availability, (kgm^{-2}), M_t is the mass available in a specific time step (kgm^{-2}), dt is the property cohesive sediment time step (s), $dt_{consolidation}$ is the consolidation time step (s), t_0 is the time at the beginning of the consolidation time step, $t_{consolidation}$ is the time at the end of the consolidation time step and r_c is the consolidation rate (s^{-1}).

Once computed the consolidation flux for sediments, the other particulate properties flux is made through computing a proportionality factor between the property mass available and the sediment mass available, likewise it is made in the erosion fluxes.

$$F_{property\ consolidation} = F_{consolidation} \times \frac{M_{property}}{M_{sediment}} \quad \text{Eq. 11-22}$$

where $F_{property\ consolidation}$ is the particulate property consolidation flux (kgm^{-2}s^{-1}), $F_{consolidation}$ is the sediment consolidation flux, (kgm^{-2}s^{-1}), $M_{property}$ is the property mass available in the bottom (kgm^{-2}, and $M_{sediment}$ is the sediment mass available in the bottom (kgm^{-2}).

11.5 Other notes

In the bottom there can be defined a wide variety of properties, particulate or dissolved. For each property, in the water column, the bottom can be seen as inexhaustible source of property mass or its availability can be limited. If it is unlimited, erosion occurs always, therefore eliminating the

need to keep track on the information on how much property mass is available. On the other hand if limitation is considered, some care is needed to handle erosion. In this case, a minimum value for mass availability must be defined. If somehow, the computed erosion flux states that more mass will be eroded than it really exists, then the erosion flux is readjusted so that all the mass available erodes and not more than it should. This way, a potential erosion flux is computed, being then limited as function of the mass available for erosion. As the variable corresponding to the erosion flux is altered in this limitation step, the output value is the erosion flux that actually took place.

A similar approach is taken into account when computing the consolidation fluxes. If the sediment compartment is being modelled and if the consolidation flux is too high, in a way that more mass than it exists is consolidated, then, this consolidation flux is corrected.

11.6 Dissolved properties fluxes

Dissolved properties can be produced in the bottom, but never remain there. This means that they are flushed to the water column as soon as they “exist”. Therefore in the bottom there is only availability to the particulate properties, being considered that the bottom interstitial water is part of the water column.

12 The Free Vertical Movement Module

12.1 Introduction

The free vertical movement module computes particulate properties vertical fluxes. It is normally used to computed settling velocity for cohesive sediment or particulate organic matter transport.

12.2 Methodology

Two different approaches are followed to compute settling velocity: a constant settling velocity and a cohesive sediment concentration dependent settling velocity. In the first case, each particulate property can have its specific and constant settling velocity. This is considered to be a reasonable approach for free settling concentrations ranges. Formulation used in Mohid regards only flocculation and hindered settling concentration ranges. The general correlation for the settling velocity in the flocculation range is:

$$W_S = K_1 C^m \text{ for } \quad C < C_{HS} \qquad \text{Eq. 12-1}$$

and in the hindered settling range is:

$$W_S = K_1 C_{HS}{}^m \left[1.0 - K_2 \left(C - C_{HS}\right)\right]^{m_1} \quad \text{for} \quad C > C_{HS} \qquad \text{Eq. 12-2}$$

where W_S (ms^{-1}) is the settling velocity, C (kgm^{-3}) is the concentration, and the subscript *HS* refers to the onset of the hindered settling (of about 2 to 5 kgm^{-3}). The coefficients K_1 ($m^4kg^{-1}s^{-1}$) and K_2 (m^3kg^{-1}) depend on the mineralogy of the mud and the exponents m and m_1 depend on particle size and shape.

13 The Hydrodynamic File Module

13.1 Introduction

In this section the hydrodynamic file module of the model *Mohid* is described. This module can be seen as an auxiliary module, which permits the user of the model *Mohid* to integrate the hydrodynamic solution in space and in time and store this solution in a file. This file can later be used to simulate longer periods, like water quality simulation which needs simulation times for at least one year.

The special integration consists in the integration of several grid cells into one single cell. This grouping can be done for any quadratic group of grid cells, like 2x2 or 3x3. This grouping results in a drastic reduction of computing points. In the case of space integration 2x2, the resulting domain will just contain one forth of grid points, each with the double size in the horizontal and vertical extension. Figure 13-1 shows a schematic representation of the space integration 2x2. The number of the overall grid points reduces from 16 to 4.

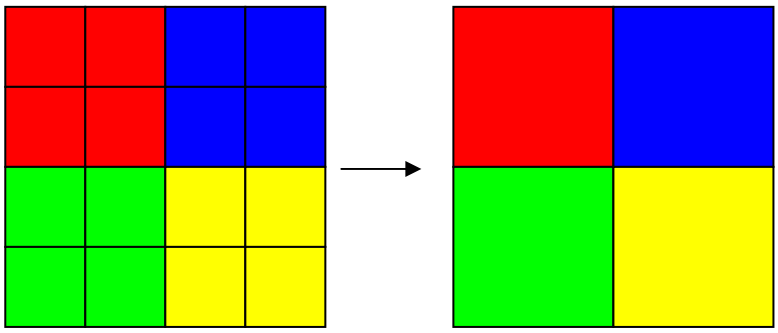

Figure 13-1: Schematic representation of the space integration

The time integration consists in the integration along several time steps of the hydrodynamic solution. The time integration can be directly connected to the space integration, once the larger grid spacing obtained by the space integration, allows the model to run with a larger time step. In the case of mass transport, the celerity which controls the stability of the model isn't the propagation of the pressure wave, but the maximum flow velocity.

In the resulting file, the hydrodynamic solution of the in time and in space integrated hydrodynamic solution is stored, which in posterior simulation can be used to obtain results more quickly. Regarding time, there are two different ways of storing this information: the information can be stored as a integrated solution with a given start date and a given end date, or as a solution which repeats itself (one tidal cycle).

The usage of the hydrodynamic file module has shown that the errors introduced in the integrated solution are usually small, and not significant for long-term water quality simulations.

The information flux of the hydrodynamic file module, relative to the other modules of *Mohid*, is shown in Figure 13-2. At the top the process of the file recording is shown and at the bottom the process of getting the solution from the file is shown.

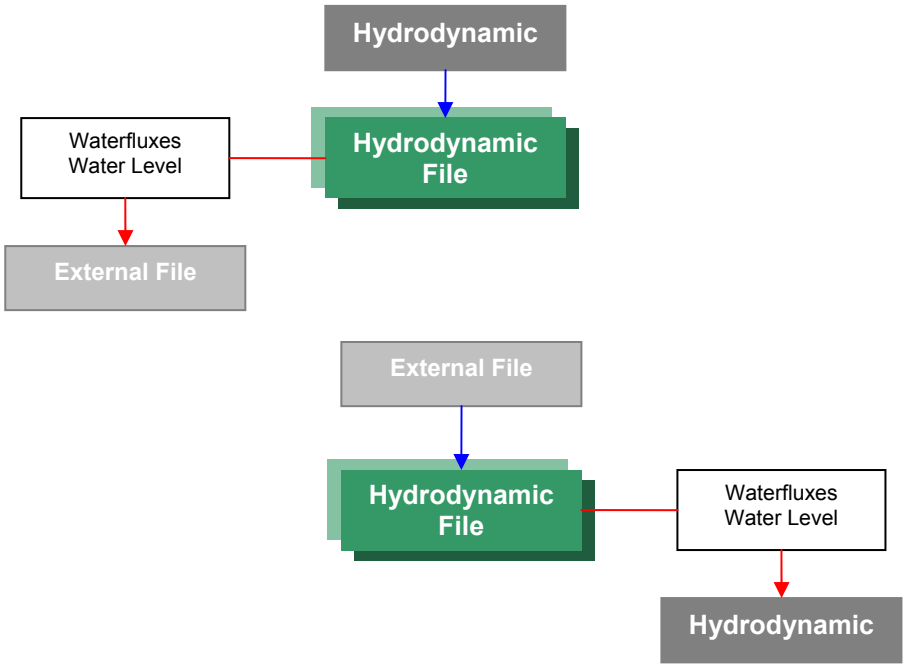

Figure 13-2: Information flux between the Hydrodynamic File Module and other modules

13.2 Methodology

The space integration is divided into to steps:

1. Compute an integrated bathymetry, base on the bathymetry with a higher resolution

2. In each integration step, the sum of all water fluxes along a given face is kept in the output file. The average surface elevation is also kept in the output file.

13.2.1 Integration of the bathymetry

The integration of the bathymetry can be done in two different ways. In both ways, before the bathymetry is integrated, the land points with are filled with the minimum depth of the cells which are to be integrated.

The first way of the integration is designated as “Mean Integration”. This methodology calculates the average depth of the cells to be integrated, using this average as the depth for the new bathymetry. Figure 13-3 shows an integration of the bathymetry by the “Mean Integration” methodology. Water points are colored blue and land points are colored grey.

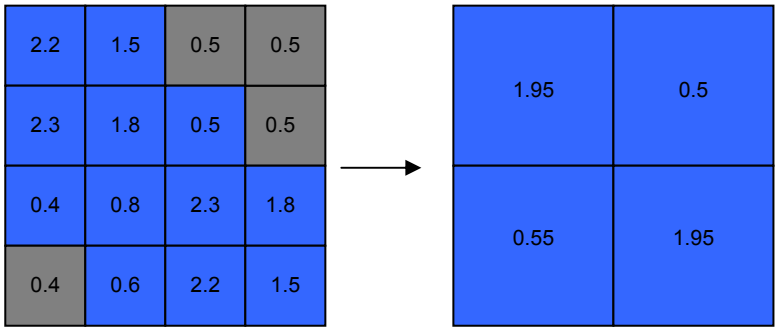

Figure 13-3: Integration of the bathymetry using the “Mean Integration”

The second way of integration is designated as “Maximum Integration”. This methodology uses the maximum depth of all cells, multiplied by the area of each cell and then divided by the total area of the water points.

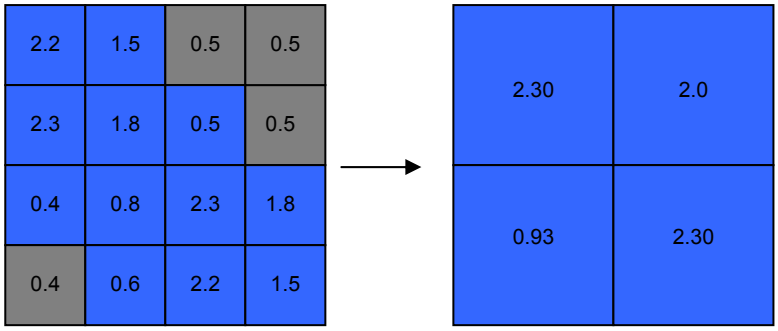

Figure 13-4: Integration of the bathymetry using the "Maximum Integration"

13.2.2 Integration of the water fluxes

The water flux between two cells is calculated from the average water flux between these cells. These fluxes can be integrated over several time steps.

$$Q_i = \sum_{1}^{nCells} \sum_{1}^{nSteps} q_i / nSteps \qquad \text{Eq. 13-1}$$

Figure 13-5 shows a schematic representation of the integrated water fluxes over the integrated bathymetry.

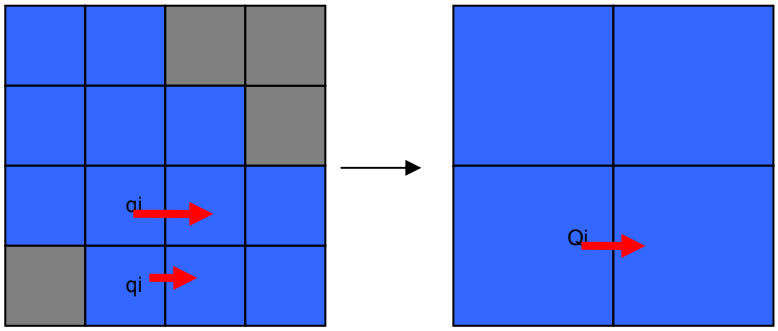

Figure 13-5: Schematic representation of the water flux integration

14 Bibliography

14.1 General Overview

Bowie, G. L., W. B. Mills, D. B. Porcella, C. L. Cambell, J. R. Pagendorf, G. L. Rupp, K. M. Johnson, P. W. Chan, S. A. Gherini, and C. E. Chamberlin (1985) – Rates, Constants and Kinetic Formulations in Surface Water Quality Modeling. U. S. Environmental Protection Agency

Braunschweig, F (2001) – Generalização de um modelo de circulação costeira para albufeiras, MSc. Thesis, Instituto Superior Técnico, Technical University of Lisbon

Cancino, L. and R. Neves (1999) - Hydrodynamic and sediment suspension modelling in estuarine systems. Part II: Application to the Western Scheldt and Gironde estuaries, J*ournal of Marine Systems* 22, 117-131

Coelho, H., A. Santos, T. L. Rosa and R. Neves (1994) - Modelling the wind driven flow off Iberian Peninsula, *GAI*A, 8, 71-78

Decyk, V. K., C. D. Norton, B. K. Szymanski (1997) – Expressing Object-Oriented Concepts in Fortran90. *ACM Fortran Forum, Vol. 16*

Leitão, P. C. (1996) – Modelo de Dispersão Lagrangeano Tridimensional. Ms. Sc. Thesis, Universidade Técnica de Lisboa, Instituto Superior Técnico

Neves, R. J. J. (1985) - Étude Experimentale et Modélisation des Circulations Trasitoire et Résiduelle dans l'Estuaire du Sado. Ph. D. Thesis, Univ. Liège

Neves, R., H. Coelho, P. Leitão, H. Martins, and A. Santos (1998) - A numerical investigation of the slope current along the western European margin. In: Burgano V., Karatzas G., Payatakas A., Brebbia C., Gray W. and Pinder G. (Ed.), Computational Methods in Water Resources XII, 2, 369-376, 1998.

Martins, F. (1999) – Modelação Matemática Tridimensional de Escoamentos Costeiros e Estuarinos usando uma Abordagem de Coordenada Vertical Genérica. Ph. D, Thesis, Universidade Técnica de Lisboa, Instituto Superior Tecnico

Martins, F., P. Leitão, A. Silva and R. Neves (2000) - 3D modeling in the Sado estuary using a new generic vertical discretization approach, submitted to *Oceanologica Act*a

Miranda, R. (1999) – Nitrogen Biogeochemical Cycle Modeling in the North Atlantic Ocean. Tese de Mestrado, Universidade Técnica de Lisboa, Instituto Superior Técnico

Miranda, R., F. Braunschweig, P. Leitão, R. Neves, F. Martins and A. Santos (2000) – Mohid 2000, A Costal integrated object oriened model. Hydraulic Engineering Software VIII, WIT Press

Montero, P., M. Gómez-Gesteira, J. J. Taboada, M. Ruiz-Villarreal., A. P. Santos, R. J. J. Neves, R. Prego and V. Pérez-Villar (1999) - On residual circulation of Vigo Ría using a 3D baroclinic model, Boletín Instituto Español de Oceanografía„n o 15. SUPLEMENTO-1

Montero, P. (1999) - Estudio de la hidrodinámica de la Ría de Vigo mediante un modelo de volúmenes finitos (Study of the hydrodynamics of the Ría de Vigo by means of a finite volume model), Ph.D. Dissertation, Universidad de Santiago de Compostela, in Spanish

Pérez-Villar, V. (1999) - ’’Ordenación Integral del Espacio Maritimo-Terrestre de Gali-cia: Modelización informática’’ (Integrated Management of the Galician Maritime-Terrestrial Space: Numerical Modelling). Final report by the Grupo de Física Non Lineal, Consellería de Pesca, Marisqueo e Acuicultura. Xunta de Galicia.

Santos, A. J. (1995) - Modelo Hidrodinâmico Tridimensional de Circulação Oceânica e Estuarina. Ph. D, Thesis, Universidade Técnica de Lisboa, Instituto Superior Técnico

Taboada J.J., R. Prego, M. Ruiz-Villarreal, P. Montero, M. Gómez-Gesteira, A. Santos and

V. Pérez-Villar (1998) - Evaluation of the seasonal variations in the residual patterns in the Ría de Vigo (NWSpain) by means of a 3D baroclinic model, Estuarine Coastal and Shelf Science 47, pp. 661-670

Taboada, J.J., M. Ruíz-Villarreal, M. Gómez-Gesteira, P. Montero, A. P. Santos, V. Pérez-Villar and R. Prego (2000) - Estudio del transporte en la Ría de Pontevedra (NOEspaña) mediante un modelo 3D: Resultados preliminares, In: Estudos de Biogeoquímica na zona costeira ibérica,Eds. A.Da Costa, C. Vale and R. Prego, Servicio de Publicaciones da Universidade de Aveiro in press.

Taboada, J.J. (1999) - Aplicación de modelos numéricos al estudio de la hidrodinámica y del flujo de partículas en el Mar Mediterráneo (Application of numerical models for the study of hydro-dynamics and particle fluxes in the Mediterranean Sea), Ph. D. Dissertation, Universidad de Santiago de Compostela. In Spanish

Villarreal, M.R., P. Montero, R. Prego, J.J. Taboada, P. Leitao, M. Gómez-Gesteira, M. de Castro and V. Pérez-Villar (2000) - Water Circulation in the Ria de Pontevedra under estuarine conditions using a 3d hydrodynamical model, submitted to Est. Coast. and Shelf Sc.

14.2 The Geometry Module

Arakawa, A. and V.R. Lamb (1977) - Computational design of the basic dynamical processes of the UCLA General Circulation Model. Methods of Computational Physics, 17, pp.174-264

Chippada S., C. Dawson, M. Wheeler, (1998) - Agodonov-type finite volume method for the system of shallow water equations, Computer methods in applied mechanics and engineering. 151(01): 105-130

Hirsch, C. (1988) - Numerical computation of internal and external flows. Vol I: Fundamentals of numerical discretization. Wiley Series in Numerical Methods in Engineering. John Wiley and Sons, 515 pp., Chichester

Martins, F. (1999) – Modelação Matemática Tridimensional de Escoamentos Costeiros e Estuarinos usando uma Abordagem de Coordenada Vertical Genérica. Ph. D, Thesis, Universidade Técnica de

Lisboa, Instituto Superior Tecnico

Martins, F., P. Leitão, A. Silva and R. Neves (2000) - 3D modeling in the Sado estuary using a new generic vertical discretization approach, submitted to *Oceanologica Act*a

Montero, P. (1999) - Estudio de la hidrodinámica de la Ría de Vigo mediante un modelo de volúmenes finitos (Study of the hydrodynamics of the Ría de Vigo by means of a finite volume model), Ph.D. Dissertation, Universidad de Santiago de Compostela, in Spanish

14.3 The Hydrodynamic Module

Abbott, M.B., A. Damsgaardand and G.S. Rodenhuis (1973) - System 21, Jupiter, a design system for two dimensional nearly horizontal flows. J. Hyd. Res, 1, 1-28

Backhaus, J (1985) - A three dimensional model for the simulation of shelf sea dynamics. Dt. Hydrogr.Z., 38, 165-187.

Fletcher, C.A.J. (1991) - Computational techniques for fluid dynamics. Volume I. 2nd Edition. Springer Series in Computational Physics, Springer Verlag, 401 pp., New York

James, I.D. (1987) - A general three-dimensional eddy-resolving model for stratified seas. In: Three-dimensional models of marine and estuarine dynamics,edited by J.C.Nihoul and B.M.Jamart, Elsevier Oceanography Series 45 Amsterdam, 1-33

Leendertsee, J.J. (1967) - Aspects of a computational model for long water wave propagation. Rand Corporation, Memorandum RM-6230-RC, Santa Monica, 1970.

Martins, F. (1999) – Modelação Matemática Tridimensional de Escoamentos Costeiros e Estuarinos usando uma Abordagem de Coordenada Vertical Genérica. Ph. D, Thesis, Universidade Técnica de Lisboa, Instituto Superior Tecnico

Montero, P. (1999) - Estudio de la hidrodinámica de la Ría de Vigo

mediante un modelo de volúmenes finitos (Study of the hydrodynamics of the Ría de Vigo by means of a finite volume model), Ph.D. Dissertation, Universidad de Santiago de Compostela, in Spanish

Palma, E. and R. P. Matano (1998) - On the implementation of passive open boundary conditions for a general circulation model: The barotropic mode. Journal of Geophysical Research, 103, 1319-1342

Santos, A. J. (1995) - Modelo Hidrodinâmico Tridimensional de Circulação Oceânica e Estuarina. Ph. D, Thesis, Universidade Técnica de Lisboa, Instituto Superior Técnico

14.4 The Lagrangian Module

Allen, C. M. (1982) - Numerical simulation of contaminant dispersion in estuary flows. Proc. R. Soc. London. A 381, 179-194 (1982).

Costa, M. V. (1991) - A Three-Dimensional Eulerian-Lagrangian Method for Predicting Plume Dispersion in Natural Waters - Diplôme d'Etudes Approfondies Européen en Modélisation de l'Environnement Marin - ERASMUS

Monteiro, A. J. (1995) - Dispersão de Efluentes Através de Exutores Submarinos. Uma contribuição para a modelação matemática. Universidade Técnica de Lisboa, Instituto Superior Técnico

14.5 The Module Oil

Buchanan I., N. Hurford (1988) - Methods for predicting the physical changes in oil spilt at sea. Oil & Chemical Pollution, 4(4), pp. 311-328

Delvigne G.A.L., C.E. Sweeney (1998) - *Natural Dispersion of Oil. Oil & Chemical Pollution*. 4, pp. 281-310

Fay J.A. (1969) - *The spread of oil slicks on a calm sea.* Oil on the Sea, Plenum Press, NY, pp. 53-63

Fingas, Mervin (1998) - *The evaporation of oil spills: development and implementation of new prediction methodology*. Marine Environmental Modelling Seminar '98, Lillehammer, Norway

Flores H., A. Andreatta, G. Llona, and I. Saavedra (1998) - *Measurements of oil spill spreading in a wave tank using digital image processing.* Oil and hydrocarbon spills, modeling, analysis and control, WIT Press, Southampton, UK, pp.165-173

Huang, J.C., F.C. Monastero (1982) - *Review of the state-of-the-art of oil spill simulation models*. Final Report submitted to the American Petroleum Institute

Leitão, Paulo (1996) - *Modelo de dispersão lagrangeano tridimensional* – dissertação de mestrado, Instituto Superior Técnico, Universidade Técnica de Lisboa, Lisboa

Mackay D., I. A. Buistt, R. Mascarenhas, S. Paterson (1980) - *Oil spill processes and models*. Environment Canada Manuscript Report No. EE-8, Ottawa, Ontario

Mooney, M.(1951) - *The viscosity of a concentrated suspension of spherical particles*, J Colloidal Science, 10, 1951, pp. 162-170

NOAA (1994) - *ADIOS™ (Automated Data Inquiry for Oil Spills) user's manual.* Seattle: Hazardous Materials Response and Assessment Division, NOAA. Prepared for the U.S. Coast Guard Research and Development Center, Groton Connecticut, 50 pp.

NOAA (2000) - *ADIOS™ (Automated Data Inquiry for Oil Spills) version 2.0.* Seattle: Hazardous Materials Response and Assessment Division, NOAA. Prepared for the U.S. Coast Guard Research and Development Center, Groton Connecticut

Payne,J.R., B.E. Kirstein, J.R. Clayton, C. Clary. R. Redding, D. McNabb, G. Farmer. (1987) - *Integration of Suspended Particulate Matter and Oil Transportation Study.* Final Report, Report to Minerals Management Service, MMS 87-0083

Proctor, R. ,R.A. Flather, A.J. Elliot (1994) - *Modelling tides and surface drift in the Arabian Gulf – application to the Gulf oil spill.* Continental Shelf Res 14:531-545

Rasmussen, D. (1985) - *Oil Spill Modelling – A tool for cleanup operations*. Proc. 1985 Oil Spill Conference, American Petroleum Institute, 243-249

Reed M. (1989) - *The physical fates component of the natural resource damage assessment model system*. Oil & Chemical Pollution, 5, pp. 99-123

Stiver W., D. Mackay (1984) - *Evaporation rate of spills of hydrocarbons and petroleum mixtures*. Environmental Science and Technology, 18(11), pp. 834-840

14.6 The Water Properties Modules

Leendertsee, J.J. and S.K. Liu (1978) – A three-dimensional turbulent energy model for non-homogeneous estuaries and coastal sea systems. Hydrodynamics of Estuaries and Fjords, J.C.J. Nihoul Ed. Elsevier Publ. Co., Amsterdam, pp. 387-405

UNESCO (1981) - Tenth Report on the joint panel on oceanographic tables and standards. Technical papers in marine science, N. 36, 24 pp

14.7 The Water Quality Module

Arhonditsis, G., Tsirtsis, G., Angelidis, M.O., Karydis, M. (2000) - Quantification of the effects of nonpoint nutrient sources to coastal marine eutrophication: application to a semi-enclosed gulf in the Mediterranean Sea. Ecological Modelling 129:. 209-227

EPA (1985) - Rates, constants, and kinetics formulations in surface water quality modeling (2nd. ed.). United States Environmental Protection Agency, Report EPA/600/3-85/040

Eilers, P.H.C., Peeters, J.C.H. (1988) - A model for the relationship between light intensity and the rate of photosynthesis in phytoplankton. Ecol. Modelling 42: 113-133

Falkowski, P.G.; Wirick, C.D. (1981) - A simulation model of the effects of vertical mixing on primary productivity. Mar Biol 65: 69-75.

Fransz, H.G., J. P. Mommaerts and G. Radach (1991) - Ecological

Modelling of the North Sea. Netherlands Journal of Sea Reserch 28 (1/2): 67-140

Humborg, C., K. Fennel, M. Pastuszak and W .Fennel (2000) - A box model approach for a long-term assessment of estuarine eutrophication, Szczecin Lagoon, southern Baltic. Journal of Marine Systems 25: 387- 403

Martins, M. & Dufner, M.J.L., (1982) - Estudo da qualidade da água. Resultados referentes às observações sinópticas em 1980. Estudo Ambiental do Estuário do Tejo (2ªsérie), nº 14. Comissão Nacional do Ambiente, Lisboa, pp.1-212

Nakata, K., F. Horiguchi, M. Yamamuro (2000) - Model study of Lakes Shinji and Nakaumi – a coupled coastal lagoon system. Journal of Marine Systems 26: 145- 169

Napolitano, E. ; Oguz, T.; Malanotte-Rizzoli, P.; Yilmaz, A.; Sansone, E. (2000) - Simulation of biological production in the Rhodes and Ionian basins of the eastern Mediterranean. Journal of Marine Systems 24: 277-298

Neumann, T. (2000) - Towards a 3D-ecosysytem model of the Baltic Sea. Journal of Marine Systems, 25: 405-419

Parsons, T.R.; Takahashi, M. & Hargrave, B. (1984) - Biological oceanographic processes, 3rd. ed., Pergamon Press, Oxford, 330 pp

Pina, P. M. N (2001) – An Integrated Approach to Study the Tagus Estuary Water Quality. Tese de Mestrado, Universidade Técnica de Lisboa, Instituto Superior Técnico

Platt, T.; Galeggos, C.L.; Harrison, W.G. (1980) - Photoinhibition of photosynthesis in natural assemblages of marine phytoplankton. J. Mar. Res. 38 :687-701

Portela, L.(1996) - Modelação matemática de processos hidrodinâmicos e de qualidade da água no Estuário do Tejo. Dissertação para obtenção do grau de Doutor em engenharia do Ambiente.Instituto Superior Técnico, Universidade Técnica de Lisboa. 240 pp

Rivera, P.C. (1997) - Hydrodynamics, sediment tranport and light extinction off Cape Bolinao, Philippines. PhD Dissertation. A.A.Balkema/Rotterdam/Brookfield

Somlyódy, L., L. Koncsos (1991) - Influence of sediment resuspension on the light conditions and algal growth in lake Balaton. Ecological Modelling, 57: 173-192

Steele, J. H. (1962) Environmental control of photosynthesis in the sea. Limnology and Oceanography, 7: 137-150

Tett, P and H. Wilson (2000) - From biogeochemical to ecological models of marine microplankton. Journal of Marine Systems, 25:431-446

Thornton, K. W. and Lessen, A. S. (1978) - A temperature algorithm for modifying biological rates. Trans. Am. Fish. Soc., 107 (2): 284-287

Valiela, I. (1995) - Marine ecological processes. Springer-Verlag, New York. 686 pp

Vila, X.,Colomer, L.J., Garcia-Gil. (1996) - Modelling spectral irradiance in freshwater in relation to phytoplankton and solar radiation. Ecological Modelling 87: 56-68

14.8 The Surface Module

Brock, T. D. (1981) - Calculating solar radiation for ecological studies. Ecological Modelling

14.9 The Bottom Module

Krone, R.B. **,** **(**1962) - Flume studies of the transport in estuarine shoaling processes. Hydr. Eng. Lab., Univ. of Berkeley, California, USA.

Partheniades, E., (1965) **-** Erosion and deposition of cohesive soils. J. Hydr. Div., ASCE, 91, No. HY1 : 105-139.